Integration of microseism, wavemeter buoy, HF Radar and hindcast data to analyze the Mediterranean cyclone Helios

Alfio Marco Borzì[1*], Vittorio Minio[1], Raphael De Plaen[2], Thomas Lecocq[2], Salvatore Alparone[3], Salvatore Aronica[4], Flavio Cannavò[3], Fulvio Capodici[5], Giuseppe Ciraolo[5], Sebastiano D'Amico[6], Danilo Contrafatto[3], Giuseppe Di Grazia[3], Ignazio Fontana[4], Giovanni Giacalone[4], Graziano Larocca[3], Carlo Lo Re[7], Giorgio Manno[5], Gabriele Nardone[7], Arianna Orasi[7], Marco Picone[7], Giovanni Scicchitano[8], Andrea Cannata[1,3]

[1]Dipartimento di Scienze Biologiche, Geologiche ed Ambientali - Sezione di Scienze della Terra, Università degli Studi di Catania, Catania, Italy;

[2]Seismology-Gravimetry, Royal Observatory of Belgium, Brussel, Belgium;

[3]Istituto Nazionale di Geofisica e Vulcanologia - Sezione di Catania, Osservatorio Etneo, Catania, Italy;

[4]Institute of Anthropic Impacts and Sustainability in the Marine Environment - National Research Council (IAS-CNR), Campobello di Mazara, TP, Italy

[5]Dipartimento di Ingegneria Civile, Ambientale, Aerospaziale, dei Materiali, University of Palermo, 90128 Palermo, Italy

[6]Department of Geosciences, University of Malta, Msida, Malta;

[7]Centro Nazionale per la Caratterizzazione Ambientale e la Protezione Della Fascia Costiera, la Climatologia Marina e l'Oceanografia Operativa, Italian National Institute for Environmental Protection and Research, Rome, Italy.

[8]Dipartimento di Scienze della Terra e Geoambientali, Università degli Studi di Bari Aldo Moro, 70125 Bari, Italy

*Corresponding author

alfio.borzi@phd.unict.it

Corso Italia 57, 95129 Catania (Italy)

Keywords: Microseism, wavemeter buoy, HF Radar, Mediterranean cyclones, climate change, monitoring sea state

Abstract

In this work, we study a Mediterranean cyclone, ~~that was~~ called Helios, ~~and~~ took place during the period 9-11 February 2023 in the southeastern part of Sicily and Malta Island, by a multiparametric approach combining microseism results with sea state and meteorological data provided by wavemeter buoy, HF Radar, hindcast maps and satellite SEVIRI images. The sub-tropical system Helios caused heavy rainfall, strong wind gusts and violent storm surges with significant wave heights greater than 5 meters. We deal with the relationships between such a system and the features of microseism (the most continuous and ubiquitous seismic signal on the Earth) in terms of spectral content, space-time variation of the amplitude and source locations tracked by means of two different methods (amplitude-based grid search and array techniques). By comparing the location of the microseism sources and the area affected by significant storm surges, derived from sea state data, we note that the microseism location results are in agreement with the real position of the storm surges. In addition, we are able to obtain the seismic signature of Helios using a method that exploits the coherence of continuous seismic noise. Hence, we show how an innovative monitoring system of the Mediterranean cyclones can be designed by integrating microseism information with other techniques routinely used to study meteorological phenomena.

1. Introduction

Significant storm surges driven by intense low-pressure systems represent one of the main hazards to the Mediterranean coastal areas causing flooding, beach erosion and damage to infrastructures and cultural heritages (Flaounas et al., 2022; Lionello et al., 2019;). Occasionally, when there are favorable conditions like high sea temperature and high contrast

of temperature sea-air, the cyclones can acquire the characteristics of a MEDIterranean hurriCANE (hereinafter Medicane). Medicanes genesis is favored when an extratropical depression gets isolated from the polar jet stream. The "cut-off" feature, when situated above the Mediterranean Sea, remains relatively stable and takes advantage of the abundant heat and humidity from the sea to generate organized convection (Faranda et al., 2022).

The structure of a Medicane is characterized by the presence of a central free-cloud “eye”, a strong rotation around the pressure minimum, an eyewall with convective cells, from which rain bands extend. It, that can be considered like a small-scale tropical cyclone, ~~and~~ can lead to sea-level rise, storm surge and sea waves that can reach significant heights of about five meters (Miglietta and Rotunno, 2019). The typical Medicane lifetime is limited to a few days, generally from 2 to 5 days, as a result of the small areal extension of the Mediterranean Sea that represents their main energy source; for the same reason also the diameter is generally restricted to a range between 100 and 300 km (Comellas et al., 2021), and their intensity rarely exceeds the category 1 of the Saffir-Simpson hurricane wind scale (Miglietta end Rotunno., 2019). In addition, due to the geometrical and meteorological characteristics of the Mediterranean Sea, a Medicane reaches fully tropical characteristics (a symmetric, deep warm-core structure and convection in their development and maintenance) for a short time, while extratropical features (non-symmetrical structure and not well-developed convection around the core) prevail for most of their lifetime (Miglietta et al., 2011, 2013). As yet, there is no clear separation between tropical and extratropical cyclones, and the first approach to differentiate these cyclones was developed by Hart (2003). This method, called cyclone phase space analysis, relies on a large spectrum of different cyclone types by using several parameters such as the symmetry/asymmetry and the cold or warm core. In this way, as explained by the author, an objective classification of cyclone phase is possible, merging the basic structural description of tropical, extratropical, and hybrid cyclones into a continuum. ~~There is no clear~~

Formatted: Font: (Default) Times New Roman, 12 pt, English (United States)

Formatted: Font: (Default) Times New Roman, 12 pt, English (United States)

~~separation between tropical and extratropical cyclones, the first approach to differentiate these cyclones was developed by Hart (2003). This method, called cyclone phase space analysis, relies on a large spectrum of different cyclone types in a way to form a continuum between tropical and extratropical cyclones.~~

The favorable months to the Medicanes generations are the autumn and early winter months (from September to January). Indeed during these months, the Mediterranean Sea preserves high temperatures after the summer season, and the first cold upper-air troughs are observed, thus creating a high sea-air temperature gradient (Cavicchia et al., 2014; Nastos et al., 2018). Specifically, the occurrence of intense convective instability is initiated when the polar jet stream transports cold air masses over the warmer Mediterranean Sea (Cavicchia et al., 2014; Nastos et al., 2018). The Medicanes generation during the late-winter months (February and March) is possible but less common (Cavicchia et al., 2014, Tous and Romero, 2013).

These Mediterranean extreme weather events caused damages, floods, deaths, and injuries in several Mediterranean coastal areas (South France, Central and South Italy, Malta, Balearic islands, Greece, Crete, Turkey, and some African states; Androulidakis et al, 2022; Bouin and Brossier, 2020; Carrió et al., 2017; Dafis et al., 2018; Di Muzio et al., 2019; Faranda et al., 2022; Kerkmann and Bachmeier, 2011; Lagouvardos et al., 2022; Pravia-Sarabia et al., 2021; Portmann et al., 2020; Rumora et al., 2018; Varlas et al., 2020; Zimbo et al., 2022). As explained by Cavicchia et al. (2014), the most frequent genesis regions are the Balearic Islands and the Ionian Sea. In particular, during the last 12 years, the majority of the Medicanes have been developed over the Ionian Sea and this is probably linked to the sea surface temperature that, as shown by Shaltout and Omstedt (2014), in the Ionian Sea is constantly 1.0°-1.5° C higher than that in the Tyrrhenian Sea.

Although these extreme Mediterranean events showed significant wave heights (hereinafter SWH, defined as the average wave height of the highest one-third of the waves), comparable

to the common seasonal storms, they caused greater coastal flooding (Scardino et al., 2022; Scicchitano et al., 2021). The strong winds, generated during a Medicane, cause the development of powerful wave motions and lead to an energy transfer from the sea waves to the solid Earth (Borzì et al., 2022). This energy transfer between the atmosphere, the hydrosphere and the solid Earth is one of the generation mechanisms of the most continuous and ubiquitous seismic signal on the Earth, called microseism (e.g. Hasselmann, 1963; Longuet-Higgins, 1950). In connection with the spectral content and the source mechanism (e.g. Haubrich and McCamy, 1969), it is possible to divide this signal into: primary microseism (PM), that shows the same period as the oceanic waves (13 - 20 s) and low amplitudes, and is generated by the energy transfer of oceanic waves breaking against the shoreline (Ardhuin et al., 2015; Hasselmann, 1963); secondary microseism (SM), generated by sea waves with the same frequency traveling in opposite directions and exhibiting frequency about twice of the frequency of the oceanic waves (period of 5 - 10 s) and amplitude higher than the PM (e.g. Ardhuin and Roland, 2012; Ardhuin et al., 2015; Lepore and Grad, 2018; Longuet-Higgins, 1950; Oliver and Page, 1963); short-period secondary microseism (SPSM), that has a period shorter than 5 seconds and is generated by the interaction between local wave motions near the coastline (Bromirski et al., 2005).

Several works deal with the relationship between microseism and the sea state (Ardhuin et al., 2019; Cannata et al., 2020; Guerin et al., 2022; Moschella et al., 2020), while others take into account specifically the relationship between microseism and cyclonic activity (e.g., Bromirski, 2001; Bromirski et al., 2005; Gerstoft et al., 2006; Gualtieri et al., 2018; Lin et al., 2017; Retailleau and Gualtieri, 2019, 2021; Zhang et al., 2010) considering in particular typhoons (Lin et al., 2017), tropical cyclones (Zhang et al., 2010), and hurricanes (Gerstoft et al., 2006). ~~Interestingly, Bromirski~~Interestingly, Bromirski (2001) and Bromirski et al. (2005)

Formatted: Font: (Default) Times New Roman, 12 pt, English (United States)

showed that the microseism bands most affected by the presence of a cyclone are the SM and SPSM ones.

For the first time, the relationship between SM, SPSM, and Medicane was analyzed by Borzì et al. (2022), who considered the Medicane Apollo to reconstruct both the seismic variation in terms of power spectral density (PSD) ~~and~~, root mean square (RMS) amplitude and the Medicane position during its lifetime by two different methods (array analysis and grid search method by means of seismic amplitude decay). In this work, we explore the relationship between microseism and the Sub-Tropical system "Helios" that occurred in the Sicily Channel during the period 9-11 February 2023 (**Figure 1**). The microseism results are integrated with wavemeter buoy, HF Radar, hindcast and satellite data (SEVIRI Images) to perform an investigation as comprehensive as possible of this extreme Mediterranean meteo-marine event.

2. Sub-tropical system "Helios" (9-11 February 2023)

During the period 9-11 February 2023, a low-pressure system, later renamed Helios, developed over the Sicily Channel due to the strong contrast between the very cold air, coming from NE (Balkans area) and the relatively warm sea surface. From satellite data, the warm core anomaly of this cyclone is evident, requisite for the development of the Medicane. However, this storm failed to become a Medicane, for which it is necessary that the cyclone maintains well-developed convection around the eye, absent in this case probably due to a little interaction between sea-air caused by sea surface temperature not suitable for the development of a Medicane (https://twitter.com/medcyclones/status/1623795373423620096?s=20~~,~~ ~~;~~ https://twitter.com/medcyclones/status/1623992335104081921?s=20~~,~~ ~~;~~ https://twitter.com/medcyclones/status/1624143740800536591?s=20~~,~~ ~~;~~ last access 23/05/2023; D'Adderio et al., 2023).

In spite of this, Helios, thanks to its proximity to the Sicilian and Maltese coasts, was able to produce damage along these areas. The effects of the sub-tropical system Helios were

Formatted: Font: (Default) Times New Roman, 12 pt, English (United States)

significant, especially in Catania, Ragusa and Siracusa provinces (located in the south-eastern part of Sicily), ~~where~~ the Sicilian Meteorological service ("Regione Siciliana—SIAS—Servizio Informativo Agrometeorologico Siciliano", http://www.sias.regione.sicilia.it/) recorded heavy rainfall, more than 200 mm/48 h and peaks of about 500 mm/48 h near Noto for the days 9-10 February 2023, heavy snowfall starting from 1200 m a.s.l. with accumulations of fresh snow on Etna thicker than two meters, strong wind gusts up to 90 km/h along the exposed coast (Davies, 2023) and severe storm surge with SWH greater than 5 meters. Similar effects were also recorded in Malta. The minimum pressure value in the cyclone eye amounted to 1002 hPa. An overview of the positions and the extension of the sub-tropical system Helios is represented in **Figure 1.**

As a consequence of the damage caused by Helios, the Regional Sicilian Government decided to require a national state of emergency for 12 months for all the municipalities of Catania, Siracusa, and Ragusa provinces and some municipalities of Messina province (https://www2.regione.sicilia.it/deliberegiunta/file/giunta/allegati/N.099_15.02.2023.pdf, last access 23/05/2023).

3. Data and Methods

We analyzed the data recorded in the period 8 to 13 February 2023 comprising the development of Helios, the climax in terms of minimum pressure value, wind velocity, precipitation intensity and SWH, and its decline.

3.1. Seismic data

We used 105 seismic stations installed along the Italian and French coastal areas, in the Sicily channel coastlines (in Malta, Lampedusa and Linosa islands), in Corsica island and along the Greek coastal areas to perform spectral analysis, localization analysis by the grid search method based on seismic amplitude decay and to obtain the seismic signature of the analyzed event

(**Figure 2a** and **Supplementary Table 1**). Three of these stations (IWAV2, IWAV3 and IWAV5) were installed as part of the i-waveNET "Implementation of an innovative system for monitoring the state of the sea in climate change scenarios" project, funded by the Interreg Italia-Malta Programme (https://iwavenet.eu/; notice 2/2019 Axis 3; project code C2-3.2-106). The aim of this project is to set up an innovative sea state monitoring network, integrating different measurement technologies, such as HF radars, seismic stations, sea level probes, wave buoys and weather stations. Additionally, 15 seismic stations, installed in the Etnean area, were used to conduct array analysis (**Figure 2b** and **Supplementary ~~table~~ Table 2**). The selected seismic stations show specific characteristics: they are i) installed near the coastal areas and ii) equipped with 3-component broadband seismic sensors.

Formatted: Font: (Default) Times New Roman, 12 pt, English (United States)

Formatted: Font: 12 pt, English (United States)

3.2. Sea state measures

In this work, we use sea state data derived from four independent methodologies. In particular, we used: i) significant wave height (SWH-Hind), provided by the hindcast maps produced by Copernicus; ii) significant wave height (SWH-Buoy), period and direction of the waves measured by the wavemeter buoy installed near Mazara del Vallo; iii) significant wave height (SWH-HF), period and direction of the waves obtained by the HF Radar installed at the Marina di Ragusa harbor; iv) SEVIRI Images to spatially and temporally track the position of the cyclone. These four different data sources have been used to both describe the sea state evolution during the Helios event, and characterize the physical state of the sea which is strictly correlated to the microseism derived outputs.

3.2.1. Copernicus Data

Regarding the description of the Helios event in terms of spatio/temporal distribution of SWH, wave period and direction over the whole domain, we referred to the "MEDSEA_HINDCAST_WAV_006_012" product, provided by the Copernicus Marine

Environment Monitoring Service (CMEMS) (Korres et al., 2019). The CMEMS product contains the hindcast maps of the Mediterranean Sea Waves forecasting system and is based on the third-generation wave model WAM Cycle 4.5.4 composed by hourly wave parameters at 1/24° horizontal resolution (Korres et al., 2019).

3.2.2 Wavemeter buoy data

Concerning the wave buoy, in **Figure 2c** we show the locations of this buoy, located offshore of Mazara del Vallo, at a depth of 85 m. The Mazara buoy is managed by ISPRA and is part of the National Wave Buoy Network (RON). The instrumental equipment consists of buoys allowing the acquisition of wave parameters in real time. The long time series represent an important heritage for the knowledge of marine phenomena affecting the Italian seas, both in terms of climatology and extreme events. The RON National Wave Network is now composed of 7 stations located off the Italian coasts for the continuous measurement of wave and meteorological parameters, such as wind direction and speed, atmospheric pressure, water surface and air temperatures, with real-time data transmission. Until 2014, the ISPRA wave buoy network was equipped with WatchKeeper™ weather wave meters manufactured by the Canadian company AXYS Ltd. (Bencivenga et al., 2012). The new meteo-marine buoys were developed, designed and built in Italy for the specific needs of ISPRA. Data are collected continuously for periods of 20-25 minutes and are provided every 30 minutes.

The parameters recorded by the wavemeter buoy and used in this study are: i) SWH (m), ii) wave mean period (s) and iii) wave mean direction (°).

3.2.3. HF Radar data

Sea state measures are also provided by the HF system located in the Marina di Ragusa harbor (**Figure 2c**) which is owned by the CNR-IAS (Consiglio Nazionale delle Ricerche - Istituto per lo Studio degli Impatti Antropici e Sostenibilità in Ambiente Marino). This HF radar is part

of the CALYPSO HF network operating in the Malta-Sicily channel since 2013. The network is nowadays composed of seven HF Codar SeaSonde systems transmitting at 13.5 MHz (central frequency). The network provides sea surface current maps at 3 km of spatial resolution at hourly scale (Capodici et al., 2019). Each HF radar provides sea state variables (SWH-HF, wave period, wave direction) every 15 minutes; these data are referred to 10 independent annular rings 3 km wide, centered at the HF site location. Data used in this work regard the last annular ring (30 km far from the HF site) showing the best temporal continuity of the measurements. The sea state derived by the HF technology has been deeply validated by several authors (e.g. Long et al., 2011; Lorente et al., 2021; Orasi et al., 2019; Saviano et al., 2019).

3.2.4. Satellite data

The passage of the Helios cyclone in the study area was tracked by means of the High Rate SEVIRI Level 1.5 Image Data. The Level 1.5 image data represents the geolocated and radiometrically pre-processed images that are prepared for subsequent processing steps, e.g. the extraction of meteorological products helpful in our case study. For further information about this methodology you can see the EUMETSAT website (https://navigator.eumetsat.int/product/EO:EUM:DAT:MSG:HRSEVIRI last access 25/05/2023). In particular, an image at 10.8 μm each 15' was downloaded and analyzed.

3.3. Spectral Analysis of Microseism

The seismic data were corrected for the instrument response and thereafter spectral and amplitude analyses were performed. For the spectral analysis, hourly spectra of the seismic signal were calculated by applying Welch's method (Welch, 1967) with time windows of 81.92 s. The hourly spectra, thus obtained, were gathered and represented as spectrograms, with time on the x-axis, frequency on the y-axis, and the $\log_{10}$ of the PSD indicated by a color scale. Some spectrograms obtained from the vertical component of 4 stations are shown in **Figure 3**.

Concerning the amplitude, we estimated hourly RMS amplitude time series for the typical microseism frequency bands: 0.2-0.4 Hz (SPSM, **Supplementary Figure 1**), 0.1-0.2 Hz (SM, black lines in **Figure 3**) and 0.05-0.07 Hz (PM, **Supplementary Figure 2**).

In addition, to show the spatial and temporal distribution of the RMS amplitude during the period under investigation, we plotted the mean RMS amplitude computed on non-overlapped 1-day-long moving windows for the three microseism bands ~~,~~ **(Figure 4, Supplementary Figures 3 and 4)**. Each dot, in **Figure 4** and in **Supplementary Figures 3 and 4,** represents a seismic station and the color of the dot relates to the corresponding RMS amplitude at that location, as specified in the color bar. Noteworthy, the colorbar of the PM band **(Supplementary Figure 3)** shows a different range of RMS amplitude highlighting a different response between the PM and the SM and SPSM bands to the sub-tropical system Helios (**Figure 4** and **Supplementary Figure 4**). Furthermore, in these figures, ~~, in this case,~~ we compared the RMS amplitude with the SWH, represented by the contour lines. A detailed description of all the figures cited in this paragraph is given in section 4.2.

Formatted: Font: (Default) Times New Roman, 12 pt, English (United States)

Formatted: Font: (Default) Times New Roman, 12 pt, English (United States)

Formatted: Font: (Default) Times New Roman, 12 pt, English (United States)

Formatted: Font: (Default) Times New Roman, 12 pt, English (United States)

Formatted: Font: Not Bold

Formatted: Font: (Default) Times New Roman, 12 pt, English (United States)

3.4 Correlation analysis between microseism amplitude and significant wave height

The calculation of correlation coefficients between the RMS amplitude time series and the significant wave height time series was conducted in accordance with previous studies (e.g., Bromirski, 2001). This calculation was performed for each grid cell of the hindcast maps during the investigated period to obtain information about the spatial variabilityof the correlation coefficients~~.~~. This kind of analysis provides information about the location of the main sources of the microseism recorded by the 4 selected stations. To explore the non-linear relationship between seismic RMS amplitudes and significant wave heights, we followed the approach proposed by Craig et al. (2016) and employed the Spearman correlation coefficient. The Spearman correlation coefficient is defined as a nonparametric measure of rank correlation (Craig et al., 2016). Correlation maps, gathering together the correlation values obtained in the

nodes of the whole Mediterranean Sea, were obtained for the vertical component of each station and the 3 typical microseism frequency bands (Figure ~~...~~5).

3. 45. Tracking Helios position by Microseism

Following Borzì et al. (2022), we used two different and complementary methods to track the position of the sub-tropical system Helios from a seismic point of view. In particular, we use i) a grid search method based on the seismic amplitude decay and ii) array analysis. These methods allow us to track the evolution over time of the location of the centroid of the seismic sources generated by the sea state variations induced by the cyclone. Such seismic data were compared with the cyclone trajectory which was identified by processing the High Rate MSG SEVIRI images. This latter task was accomplished by visually identifying the positions of the cyclone's eye which was clearly identifiable only between 01:00 and 23:00 of the 10 February 2023.

3.45.1. Grid search method

We used the seismic signals recorded by 105 seismic stations (**Figure 2a**) to map out the position of Helios during the analyzed period by employing a grid search approach (**Figure ~~5~~6**). The region, where we executed the grid search, is a bi-dimensional area of 1760 km x 2400 km (minimum longitude: 5°; maximum longitude: 30°; minimum latitude: 30°; maximum latitude: 46°) with a spacing of 1°. As shown by several authors who used seismic amplitude decay methods, both to locate microseism sources (Borzì et al. 2022) and seismo-volcanic sources (Battaglia and Aki, 2003; Cannata et al., 2013; Kumagai et al., 2011), the grid spacing is chosen as a compromise between good spatial resolution and reasonable computation time. The microseism source is localized based on the goodness of the linear regression fit (hereafter referred to as R^2) computed for each node of the bi-dimensional (2D) grid previously mentioned. Specifically, the source was identified at the centroid position of all the grid nodes

where the R2 values deviate by no more than 1% from the maximum R2 value. In this method, we used an RMS signal window of 4 hours and thus we were able to obtain 1 localization every 4 hours. In addition, following Borzì et al. (2022), we applied a method to evaluate the statistical significance of the retrieved maximum R^2 value and to test the confidence of the location results. Specifically, we conducted 20 iterations by randomly rearranging the RMS amplitude values among the stations. Then, we calculated the 95th percentile and we obtained a value of 0.27. In accordance with this result, we consider reliable the localizations with R^2 values greater than 0.27. To retrieve the errors associated with each localization, the bootstrap technique is used (Johnson, 2001). This technique consists in recalculating each source location 1000 times, by randomly resampling the data (amplitude-distance pairs) with repetition.

It must be underlined that the grid search method used in this study shows various limits that in specific cases can invalidate the source locations. In particular, the first limit concerns the fact that in this method we consider the microseism source as a point-like source, while the microseism is produced in a wide area of the Mediterranean Sea. In this scenario, the localization of the point-like source is determined as the barycentric point of the extended source. However, it is important to consider a limitation of this method related to the presence of multiple sources with similar amplitude in the same frequency range. In such cases, the constrained source location shifts towards a position between the actual seismic source locations (Battaglia et al., 2005), resulting in a significant decrease in R^2. In our case, we neglect localization showing R^2 values smaller than 0.27, to avoid unreliable localization.

3.45.2. Array analysis

In order to track the location of the sub-tropical system Helios using array techniques, we considered fifteen stations belonging to the Mt. Etna seismic permanent network and used them as a roughly circular array (**Figure 2b**).

Formatted: Font: (Default) Times New Roman, 12 pt, English (United States)

Formatted: Font: (Default) Times New Roman, 12 pt, English (United States)

Formatted: Font: (Default) Times New Roman, 12 pt, English (United States)

Formatted: Superscript

The Array Response function (ARF) is a good tool to plan the array geometry required to investigate microseism signals or, in this case, to evaluate the performance of a pre-existing array in microseism studies. The ARF, previously obtained by Borzì et al. (2022), exhibits that the roughly circular array has a good response for the PM and SM cases.

In this study, we employed the f-k (frequency-wavenumber) analysis technique on microseism signals (e.g. Rost and Thomas, 2002). This approach involves a spectral domain beamforming method that utilizes a grid search of slowness to determine the back azimuth and apparent velocity values that maximize the amplitude of the combined array traces. The result of the f-k analysis is the PSD as a function of slowness. In accordance with Borzì et al. (2022), we followed the subsequent processing steps to implement array analysis on microseism~~ic~~ data: (i) demeaning and detrending; (ii) applying a specific frequency band filter for microseism; (iii) segmenting the data into tapered windows of 120 seconds each; (iv) excluding windows containing seismo-volcanic amplitude transients (such as volcano-tectonic earthquakes, long-period events, and very long-period events) identified using the STA/LTA technique (e.g., Trnkoczy, 2012); (v) performing f-k analysis for each window by conducting a slowness grid search (ranging from -1 to 1 s/km in the east and north components of the slowness vector) with a spacing of 0.05 s/km. An illustrative example of the outcomes is presented in Figure ~~5~~6. For further details about these two methods used in this work, you can see Borzì et al. (2022).

3.~~5~~6. Seismic signature of the Medicanes

In a way to obtain the seismic signature and the main spectral characteristics of the sub-tropical system Helios, we use a method developed by Soubestre et al. (2018). This method was initially developed as a network-based method to detect and classify seismo-volcanic tremors. The proposed method utilizes the coherence of tremor signals within the network, which is determined based on the array covariance matrix. Using this technique, as explained by

Soubestre et al. (2018), it is possible to highlight both volcanic tremors and other types of seismic sources such as tectonic earthquakes (local, regional, and teleseismic), and oceanic seismic noise (microseism). This method allows the identification of the spatially coherent individual noise source within a specific network, identified as small spectral width, as opposed to other noises such as local effects that would generate multiple individual sources. For further details about the method, see Soubestre et al. (2018).

In this study, we are interested in detecting the microseism produced by the sub-tropical system Helios. Since we are interested in such a microseism, we filtered the signal in the band 0.1-1 Hz and resample it to 25 Hz in a way to reduce the computation time. To compute the covariance matrix we use only the vertical component of the seismic signal and a window length of 60 seconds. The analyses were performed using the data recorded by a station set comprising both stations installed near the south Sicilian coast (CLTA and IWAV5) and in the Malta (MSDA) and Linosa (LINA) islands in order to have the microseism source within the selected station set.

4. Results and Discussion

We analyze the sea state, derived by four independent techniques, and the seismic data recorded by the i) 105 seismic stations represented in **Figure 2a** and by ii) the 15 Etnean seismic stations (**Figure 2b**) during the period 8-13 February 2023. We chose a period longer than the real lifetime of the sub-tropical system Helios in a way to include the development, the climax in terms of meteorological events that occurred during the days 9-10 February, and the following loss of intensity.

4.1. Sea state

In **Figure ~~6~~7**, we show the SWH, the mean wave period and the direction time series recorded during the period 8-13 February 2023 by the buoy of Mazara del Vallo (**Figure ~~6b~~7b, d and f**) and the HF radar installed in Marina di Ragusa harbor (**Figure ~~6a~~7a, c and e**).

The buoy data indicates that the sea storm reached its maximum significant wave height of 3.1 m at 20:00 on 9 February, with a mean direction of 140° indicating that waves were generated by Scirocco wind, which is the main wave direction for the period under investigation and a period that varies from 5 to 9 s. The data from HF Radar, installed closer to the cyclone position than the buoy, show a maximum SWH of about 6 m recorded on 9 February at 22:30, the mean wave direction was of 100° approximately and the period varies in the range of 5-12 s. Both datasets allowed defining the time interval of the wave storm which spanned between 8-13 February 2023. The higher SWH measured by the HF radar agrees with the shorter distance from the cyclone eye (~90 km) of this instrument compared to that of the wave buoy (~190 km).

The spatio-temporal distribution of the SWH in the whole area is shown by the hindcast maps in **Figure ~~7~~8**. Noticeably that the stronger effect of the sub-tropical system Helios on the sea state of the Malta-Sicily channel was the increase of the SWH during 9 - 10 February. On 9 February the higher SWH values were recorded mainly in the patch of the sea at the east of Sicily Island and of the Maltese archipelago, whereas the wave storm invaded the whole Malta-Sicily channel on 10 February. Finally, on 11 February the wave storm started moving to the south, reaching the northern part of the African coasts.

The comparison between SWH-Hind and SWH-HF revealed a good agreement (R^2~0.85) even if an underestimation of the event by the CMS model (slope of ~0.7) was observed (~~**Supplementary Figure 5**~~**Supplementary figure 6**).

4.2. Spectral Analysis and RMS spatial distribution

To perform the spectral analysis, we used the 105 seismic stations installed along the Italian, Greek and Maltese coastal areas. In **Figure 3,** we plot the spectrograms and the RMS amplitude time series (black lines), obtained by analyzing the vertical component of the seismic signals recorded by four stations installed in Malta (MSDA **Figure 3a**), on Linosa Island (LINA **Figure 3b**), near Pozzallo (IWAV5 **Figure 3c**) and in Central Italy (CELB **Figure 3d**). We chose these four stations to compare the results obtained from the stations installed near the sub-tropical system (LINA, MSDA and IWAV5), with the result obtained from the far station (CELB).

As shown by Borzì et al. (2022), in the spectrograms a great part of the energy is focused in the 0.1-1 Hz band, corresponding with the SM and SPSM bands. In addition, it is also evident how the considered stations show a different behavior, in terms of both spectrograms (**Figure 3**) and RMS amplitude time series (**Figure 3** and **Supplementary Figures 1** and **2**), that depended on their position. In particular, spectrograms and RMS amplitude time series obtained from the data recorded by MSDA (**Figure 3a** and **Supplementary Figure 1a** and **2a**), LINA (**Figure 3b** and **Supplementary Figures 1b** and **2b**) and IWAV5 (**Figure 3c** and **Supplementary Figures 1c** and **2c**) stations, installed close to Helios (**Figure 1** and **Figure 2**), show the maximum PSD and RMS amplitude values during the time interval 9-11 February 2023, highlighted by the vertical dashed lines in **Figure 3**. On the other hand, the spectrogram and RMS amplitude time series of the station CELB (**Figure 3d** and **Supplementary Figures 1d** and **2d**), installed in the Tyrrhenian area, exhibited the maximum PSD and RMS amplitude values a few days before Helios at the same time as a local storm surge.

To show the space-time distribution of the RMS amplitude, we calculate the daily RMS average for the three main microseism bands (PM and SPSM in **Supplementary Figures 3** and **4**, SM in **Figure 4**) during the period 8-13 February 2023. All the three analyzed microseism bands

show a relationship with the position of Helios indicated by the five-pointed red star (**Figure 4c** and **Supplementary Figures 3c** and **4c**). In particular, on 10 February 2023, when Helios reached its climax, the maps in **Figure 4c** (SM) and **Supplementary Figures 3c** and **4c** (PM and SPSM respectively) show a cluster of high RMS values for the stations installed near the sub-tropical system Helios, highlighting a good match between the SM, SPSM, PM and Helios positions.

Comparing the ~~results~~ RMS amplitude time series obtained for the sub-tropical system Helios ~~with the results~~with those obtained for the Medicane Apollo (Borzì et al., 2022), we observe a similar trend for the SM and SPSM bands and a different behavior for the PM band. In particular, during the Medicane Apollo, the analysis showed a significant amplitude increase for the SM and SPSM bands while no significant changes for the PM band were observed. ~~did not show a significant amplitude increase in the PM band, while~~ Instead, ~~the analysis did not show a significant amplitude increase in the PM band, while~~ during the sub-tropical system Helios, the RMS amplitude time series for the PM (**Supplementary Figure 2**), although with two orders of magnitude smaller, showed a trend similar to the SM (**Figure 3**) and SPSM (**Supplementary Figure 1**) ones. Also the space-time distribution shows a good match between the PM (**Supplementary Figure 3**) and Helios position (**Figure 1**, **4c** and **Supplementary Figures 3c** and **4c**), even if for this band there are stations installed in central Italy that show high RMS amplitude values related to a very local storm surge that occurred at the same time as Helios.

The involvement of the PM band in the case of the sub-tropical system Helios can be explained by considering the position of this low-pressure system (**Figure 1**) and comparing it with the Apollo position. Indeed, the Medicane Apollo develops and moves in the Ionian Sea (**Figure 2**) in an area with a sea depth greater than 2000 m, while the sub-tropical system Helios develops and moves largely in the Sicily Channel, a shallower sea with a depth that reaches a

Formatted: Font: (Default) Times New Roman, 12 pt, English (United States)

maximum depth of 500 m b.s.l. and an average depth of 316 m b.s.l. In addition, the average depth between Sicily and Malta is about 65 m b.s.l. As outlined in the literature (Bromirski et al., 2005), the production of the PM is hindered in large water depths due to the attenuation of pressure fluctuations, which generate the signal, as a result of depth-dependent amplitude decay. More specifically, the PM is generated solely in depths less than half of the wavelength (where λ represents the wavelength of the oceanic waves generating the pressure fluctuations). If we consider, for the Catania and Mazara areas, a mean waves period of 6.1 and 5.6 s and a peak waves period of 9.7 and 9 s respectively (Agenzia per la Protezione dell'Ambiente e per i Servizi Tecnici Dipartimento Tutela Acque Interne e Marine Servizio Mareografico - Atlante delle onde nei mari italiani), by utilizing the correlation that connects period and wavelength ($\lambda=gT^2/2\pi$ with g acceleration of gravity that is 9.8 m/s^2 and T the period of the waves; Sarpkaya and Isaacson, 1981) we obtain a wavelength, for this part of the Mediterranean sea, ranging between ∼45 m and ∼150 m. Considering these wavelengths, the shallow depth of the Sicily Channel, especially in the Malta Channel where the average depth is about 65 m b.s.l., and the fact that the generation of the PM occurs only for depths less than ½ λ (Bromirski et al., 2005), we can remark that the generation of the PM is possible in the Sicily Channel, while can not occur in the Ionian Sea except in limited areas near the coastline. This is evident in our analysis, and in particular in the RMS amplitude time series. Indeed in the sub-tropical system Helios case, which occurred in the Sicily Channel, we can note a similar trend between the three analyzed microseism bands (**Figure 3** and **Supplementary Figures 1** and **2**), while in the case of the Medicane Apollo, that developed in the Ionian Sea (Borzì et al., 2022), we observe an RMS amplitude increase only for the SM and SPSM bands and no significant variations in the PM bands.

4.3. Comparing the RMS amplitude with the SWH

As mentioned before, microseism is a continuous seismic signal linked to the hydrosphere-solid Earth energy transfer and, as demonstrated by several authors (e.g. Ardhuin et al., 2012; Bromirski et al., 1999; Bromirski et al., 2005; Cutroneo et al., 2021; Ferretti et al., 2013, 2018), the amplitude of this signal is strictly related to the sea state and in particular to the SWH. To analyze the relationship between microseism and SWH, we plot in **Figure** ~~**8a**~~ **9a** the RMS amplitude time series for the station IWAV5 and the SWH time series derived from both HF Radar (SWH-HF) and hindcast maps (SWH-Hind), and in **Figure 5** the results of the correlation analysis between the RMS amplitude time series and the significant wave height (the position of the seismic stations IWAV5, LINA, MSDA and CLTA ~~(the position of IWAV5~~ and HF radar are respectively shown in **Figure** 2a and **2c**). The sea state information provided by the Mazara del Vallo buoy was not taken into account in this analysis because of the long distance between this instrument and the cyclone eye. We chose stations IWAV5, LINA, MSDA and CLTA both because they are some of the nearest stations to the cyclone eye and since these stations were used for the seismic signature analysis. In addition, ~~station IWAV5 because it is one of the nearest stations to the cyclone eye. Also,~~ as it is possible to see in **Figure 3a, b** and **c**, all the seismic stations installed in the Sicily Channel area show very similar microseism amplitude patterns. The time series of SWH-Hind was obtained by computing the median value of the SWH data within a wide area of the Sicily Channel shown in **Figure** ~~**8d**~~**9d**. In general, the three datasets exhibit a good agreement among them. In particular, we observe an increase that occurs almost simultaneously for SWH-HF, SWH-Hind and the RMS amplitude. However, from the first hours of 10 February, the SWH-HF started showing a different behavior compared to SWH-Hind; indeed, the SWH-HF decreased while the SWH-Hind continued to show high values up to the end of 10 February. This difference can be explained by considering that the HF Radar provides information about the SWH for a limited

Formatted: Font: Not Bold

area while SWH-Hind gives median information about a wide area of the Sicily Channel. It is interesting to note that the microseism amplitude follows more closely the areal sea state, shown by the SWH-Hind series, than the punctual one, shown by the SWH-HF. We can note this in both a qualitative way in the time series of **Figure** ~~8a~~ 9a and a quantitative way in the cross-plots of **Figures** ~~8b~~ 9b and **c**. For both the cross-plots we calculated the R^2 value, to evaluate the goodness of the linear regression, and we obtain R^2 values equal to 0.68 and 0.85, for the cross-plot RMS amplitude vs SWH-HF and RMS amplitude vs SWH-Hind, respectively. The higher value of R^2 for the RMS amplitude - SWH-Hind relationship can be explained by considering that microseism recorded by a seismic station is generated by multiple extended sources distributed on a wide portion of the sea. The correlation analysis confirms a good match between the spatial distributions of SWH and RMS amplitudes recorded by the 4 aforementioned stations during the period under investigation (**Figure 5)**. Values of the correlation factor higher than 0.85 were observed for the SM and SPSM bands for the area of the Sicily Channel and Ionian Sea affected by the storm surge ~~and~~due to the cyclone Helios.

4.4. Localization analysis

As concerns the microseism source location, we performed the location analysis for the PM, SM and SPSM using both the array techniques and the grid search method based on the seismic amplitude decay. Concerning the array techniques, we chose to focus on ~~the~~ PM and SM bands since, according to the information from the ARF, we expect reliable localizations only ~~on the PM and SM~~ for these two bands, while for the SPSM band appears spatial aliasing. As for the grid search method, we obtained reliable locations only for the SM and SPSM bands, while for the PM band, although we got localizations in agreement with the cyclone position, the associated R^2 values turned out to be slightly lower than the threshold from which we can consider the locations reliable.

By the grid search method, we obtained reliable locations from 9 February 2023 at 8:00 to 11 February 2023 at 00:00 (~~**Supplementary Figure 6**~~**Supplementary figure 7**). In agreement with satellite images (**Figure 1**), on 9 February 2023, the sub-tropical system Helios was not yet well-developed and did not show the cyclone eye. Indeed, during this day, we are able to locate a storm surge, probably linked to the primitive formation of Helios, that occurred in the Ionian Sea. In particular, our localizations, on 9 February from 8:00 to 20:00, indicate the source position near to the south-eastern part of Sicily in agreement with the hindcast data showing for this area SWH greater than 5 meters (**Figure 4b and 7**). During the following hours, our localizations (~~**Supplementary Figure 6**~~**Supplementary figure 7**) show a small but continuous shift of the source toward the Malta area (**Figure** ~~5~~**6**), in agreement with the relatively stable position of the cyclone eye for the first hours of 10 February 2023, retrieved from SEVIRI data (**Figure 1**). Successively, the sub-tropical system rapidly loses its strength and runs out completely on the day of 11 February 2023, making landfall against the Libyan coast. The errors associated with the localization show an anti-correlation with the R^2 (**Supplementary Figure 5**). In particular, we can observe errors that vary from 535 to 210 km for the longitude and from 245 to 165 km for the latitude. In particular, we obtained lower errors during the climax of Helios, when the R^2 reached the highest values~~the R^2 reached the highest values~~, and higher during the initial and final phases of the phenomenon (**Supplementary Figure 5 and Table 1**).

In **Table 1** we summarised the main features of the microseism source located by using the grid search method during the days 9-10 February 2023 and compared these with the results obtained during the period 01:00 - 23:00 of 10 February 2023 in terms of the coordinates of the cyclone eye retrieved by SEVIRI data. During the first hours of the cyclone life, the coordinates of the cyclone eye and the microseism source show only a small offset that, as explained in section 3.4.1, can be due to the fact that the point-like microseism source corresponds with the

Formatted: Superscript

Formatted: Font: Bold

Formatted: Font: (Default) Times New Roman, 12 pt, English (United States)

Formatted: Font: (Default) Times New Roman, 12 pt, English (United States)

Formatted: Font: (Default) Times New Roman, 12 pt, English (United States)

Formatted: Font: (Default) Times New Roman, 12 pt, English (United States)

barycentric position of an extended source and it is expected that the microseism source location could differ from the cyclone eye. During the following hours, as shown in **Figure 1,** the cyclone moved southward until the time when the cyclone made landfall against the Libyan coast. This shift is not visible in the microseism location results, probably due to the lack of seismic stations in Africa, that would help locate more accurately seismic sources placed close to the African Coastlines. In ~~Supplementary Figure 7~~Supplementary figure 8 we plot the temporal distribution of the R^2 values and compare this with the SWH-Hind time series. These two datasets show a good agreement and highlight that the higher R^2 values obtained from the grid search method are influenced by the presence of the sub-tropical system Helios.

Concerning the array analysis, the result obtained for the PM band shows that, for the period 9-11 February, the back azimuth values pointed toward the Ionian Sea (~~Supplementary Figure 8~~Supplementary figure 9) with apparent velocity values of ~ 3.0 km/s (~~Supplementary Figure 9~~Supplementary figure 10). For the same days, the back azimuth values for the SM band pointed toward the same region (~~Supplementary Figure 10~~Supplementary figure 11), with apparent velocity values of ~ 2.0 km/s (~~Supplementary Figure 11~~Supplementary figure 12).

For the PM and the SPSM bands, we obtained reliable locations only by one of the two used methods (array technique for the PM and grid search method for the SPSM), while for the SM we obtained reliable locations from both the aforementioned methods and we can compare the results obtained independently from these two methods. We can observe that the grid search method based on the seismic amplitude decay is able to detect both the storm surge that occurred in the Ionian sea and the following formation of the sub-tropical system Helios (~~Supplementary Figure 6~~Supplementary figure 7), and in particular by this method, we localize the cyclone as a point-like source, considered as a barycentre of an extended source. The array technique instead provides back azimuth values pointing toward the Ionian Sea for

the entire period of 9-11 February (~~Supplementary Figure 10~~Supplementary figure 11). From these results, we can note that the two methods are influenced by different sources. This different result can be explained based on the spatial station distribution. Indeed, if we consider the grid search method we use a wide station network including stations installed near the sub-tropical system Helios (MSDA, CLTA, IWAV5, LINA and other stations), while the Etnean array includes 15 stations clustered in a small area. In addition, the distance array center-Ionian Sea (~20 km) is smaller than the distance array center-Sicily Channel (~90 km). During the period taken into account, we have the coexistence of two strength sources, the first in the Ionian Sea (storm surge with SWH greater than 5 m) and the other, probably the strongest, in the Sicily Channel (Helios), both represented by the red contour line in **Figure 4c**. Hence, the coexistence of two sources and the great difference in distance between the array center and the Ionian Sea and the array center and the Sicily channel does not allow us to locate the sub-tropical system Helios with the array technique, which gives us back azimuth values pointing always toward the nearest source.

4.5. Seismic signature

To show the main spectral characteristics of the sub-tropical system Helios, we used the method developed by Soubestre et al. (2018). From our analysis, the evolution in time of the microseism spectral characteristics between the first 24 hours and the following ones is evident (**Figure ~~9~~10**). In particular, with the vertical dashed lines in **Figure ~~9~~10,** we show the time interval when Helios develops, reaches the climax and loses power to run out. The first 24 hours are characterized by the lack of a clear predominance of a particular frequency range. Starting from early 9 February 2023 (first vertical white dashed line), we can observe high coherence values clustered on a narrow frequency range between about 0.14 and 0.25 Hz, and this frequency range is constant until the 80 hours (vertical black dashed line) corresponding to the morning of 11 February. Successively, the frequency with the highest coherence starts

588 to increase reaching a value of about 0.35 Hz before the exhaustion of the phenomenon. This
589 increase in the frequency could be related to the landfall of Helios against the Lybian coast
590 (https://twitter.com/medcyclones/status/1624143740800536591?s=20, last access 23/05/2023
591). Indeed, as described in the literature (Gerstof et al., 2006; Lin et al., 2017; Sun et al., 2013),
592 there exists a relationship between the frequency, the sea depth and the development of local
593 wave motion near the coastline. In particular, Gerstof et al. (2006) show an increase in the
594 microseism frequency during the two landfalls of Hurricane Katrina. Similar results are shown
595 by Sun et al. (2013), who highlighted an increase in the intensity of the microseism for the SM
596 and SPSM and the frequency increase from the SM band toward the SPSM one during the
597 approaching of the three analyzed typhoons against the Chinese coast. Finally, Lin et al. (2017)
598 show an increase in the microseism frequency during the first landfall of typhoon Megi.
599 Similarly, we obtained an increase in frequency during the time interval when Helios
600 approached the Lybian coastline and made landfall on 11 February
601 (https://twitter.com/medcyclones/status/1624143740800536591?s=20, last access
602 23/05/2023). We were also able to observe the gradual loss of power of the sub-tropical system
603 highlighted by ever-lower coherence values until its disappearance.

604 **5. Conclusions**

605 Several works have dealt with the relationship between microseism and several meteorological
606 phenomena, considering in particular storm surges (Ardhuin et al., 2019; Cannata et al., 2020;
607 Guerin et al., 2022; Moschella et al., 2020) and different types of cyclones (Borzì et al., 2022;
608 Bromirski, 2001; Bromirski et al., 2005; Gerstoft et al., 2006; Gualtieri et al., 2018; Lin et al.,
609 2017; Retailleau and Gualtieri, 2019, 2021; Zhang et al., 2010) that affect various parts of the
610 world (hurricanes, typhoons, tropical cyclones and medicanes). In this work, we analyzed the
611 relationship between the three main microseism bands (PM, SM and ~~SPSM) and~~SPSM) and
612 the sub-tropical system Helios that occurred in the Mediterranean Sea during the time interval

9-11 February 2023. Although all the meteorological parameters suggest that Helios has not been able to reach the fully Medicane characteristics, remaining a rather weak sub-tropical system, the proximity of this cyclone to the southeastern Sicilian and Maltese coastal area has caused heavy rainfall, strong wind gusts and violent storm surge in the two above mentioned areas.

To obtain information about the sea state we take into account the data of hindcast maps, wavemeter buoy, HF radar and SEVIRI images. The first three methodologies show an increase in the SWH during the period under investigation, with a climax during the days 9-10 February 2023, due to the presence of the sub-tropical system Helios. In particular, the HF radar and the hindcast maps exhibit an SWH of about 6 meters while the wavemeter buoy shows an SWH of about 3 meters. This difference is only linked to the position where the two instruments are installed, indeed the HF radar is installed at about 90 km from the cyclone eye while the wavemeter buoy is installed at about 190 km. The last method based on SEVIRI images provide information about the location of the cyclone eye that is clearly visible between 01:00 and 23:00 on 10 February 2023.

To analyze this meteorological phenomenon from a seismic point of view, we selected 120 seismic stations installed along the Italian, Maltese and Greek coastal areas: i) 105 were used in spectral and amplitude analysis, in the grid search method and 4 of these to obtain the seismic signature of Helios using the method of the covariance matrix; ii) 15 were employed in array analysis. The results, obtained from the spectral analysis, highlight that the seismic signals, in particular the PM, SM and SPSM bands, are affected by the storm surge and by the sub-tropical system Helios. This is evident considering the RMS amplitude time series, the spectrograms and the RMS amplitude space-time distribution, in which it is possible to observe that the amplitude of the microseism signal, in the three main bands above mentioned, shows a similar trend and it is greater during the period 9-10 February 2023 for the stations installed close to

638 the Sicily Channel (for example the stations MSDA, LINA and IWAV5), while the stations
639 installed farther from Helios (for example CELB) show a different behavior conditioned by
640 local sources. Furthermore, the increase of the RMS amplitude for the PM band can be
641 explained on the basis of the position where Helios develops. Indeed, as explained in the
642 literature (Bromirski et al., 2005), the generation of the PM is limited in the areas where the
643 depth of the sea bottom is smaller than ½λ (where λ is the wavelength of the sea waves) as a
644 consequence of the amplitude decay of the pressure fluctuations. The Sicily Channel and in
645 particular the area between Malta and Sicily (Malta Channel), where Helios stood still for the
646 entire 10 February 2023, shows an average depth of about 65 m b.s.l., and considering
647 wavelength between ∼45 m and ∼150 m it is possible the generation of the PM for this area.
648 By comparing the SWH recorded by HF Radar, SWH retrieved by hindcast data and the RMS
649 amplitude recorded at the station IWAV5, we observe that the RMS amplitude time series
650 shows a trend more similar to that of hindcast data than to the HF Radar data. This could be
651 explained by considering that the microseism is a seismic signal generated by multiple and
652 extended sources in a large area of the sea and hence its amplitude is related to the state of a
653 wide portion of the sea. Also, the correlation analysis confirms a good match between the
654 spatial distributions of significant wave heights and seismic RMS amplitudes.
655 We used two different methods to track the position of the sub-tropical system Helios during
656 its lifetime and, through the performed analysis, we were able to locate both the storm surge
657 that occurred in the Ionian Sea and Helios. In particular, using the grid search method based on
658 the seismic amplitude decay we located the storm surge in the Ionian Sea on 9 February 2023
659 and the sub-tropical system Helios on the next day, while with the array technique, we located
660 only the storm surge in the Ionian Sea as a consequence of the position of the array closer to
661 the Ionian Sea than to the Sicily Channel. The location obtained both for the storm surge and
662 for the sub-tropical system Helios, during the first hours of its life, is in agreement with the real

Formatted: Normal (Web)

position of the two meteorological phenomena shown by the hindcast maps and satellite images. Successively, the sub-topical system Helios moved southward until the time when the cyclone made landfall against the Libyan coast while the microseism source continued to show a stable position near Malta Island. This difference between the two positions is probably due to the lack of seismic stations in Africa, that does not locate accurately microseism sources placed close to the African Coastlines. In addition, using the method of the covariance matrix, we obtained the seismic signature of the sub-tropical system Helios. In particular, during the development and climax of the cyclone Helios, we can observe high coherence values clustered on a narrow frequency range between about 0.14 and 0.25 Hz that, as described in the literature, corresponds to the microseism bands (SM and SPSM) most affected by cyclonic activity. This narrow frequency range stays constant until the time when Helios makes landfall when we observe an increase in the frequency until a value of about 0.35 Hz probably linked to the decrease of the sea depth and the development of local wave motion near the coastline.

Starting from Borzì et al. (2022), this work aims at studying and monitoring the Mediterranean cyclones through microseism and its integration with sea state data. It underlines that it is possible to extract information about these meteorological phenomena by an innovative system for the sea state monitoring that includes not only the classical instruments (such as wavemeter buoys, radar HF and geostationary satellites) but also seismometers. In particular, the large number of broadband seismic stations, installed for earthquake and volcanic monitoring, can compensate for the lack of data of the classical instruments mentioned above, more often affected by instrument breakage.

Finally, since we obtained the seismic signature of this particular Mediterranean cyclone we can compare it with the seismic signature of other Mediterranean events (Medicane and common storms) to identify the similarities and differences in the spectral content of different Mediterranean cyclones and other more common events. The characterization of the seismic

signature of these events could be useful to identify Mediterranean cyclones by old seismograms, and hence to reconstruct the temporal variability (in terms of occurrence rate and intensity) of these extreme meteo-marine events whose evolution seems to be strictly linked to the global warming (e.g. Emanuel, 2005; Reguero et al., 2019).

Data availability

The seismic data, in the miniseed format used in this study, can be downloaded through the ORFEUS-EIDA database (http://www.orfeus-eu.org/data/eida/). All the seismic stations used in this study, along with their main features, are reported in Supplementary Tables 1 and 2. The hindcast data are available online on the Copernicus site (https://resources.marine.copernicus.eu/products). The Italian buoy data (Mazara del Vallo) are available on the ISPRA website (https://dati.isprambiente.it/) and on the MAREOGRAFICO website (www.mareografico.it). Satellite data are available on the EUMETSAT website (https://navigator.eumetsat.int/product/EO:EUM:DAT:MSG:HRSEVIRI). The HF Radar data are available on the CALYPSO project website by compiling the form indicated on the web page (https://www.calypsosouth.eu/index.php/welcome/open_page/50/0) or by contacting giuseppe.ciraolo@unipa.it or salvatore.aronica@cnr.it.

Acknowledgments

The authors thank the i-waveNET "Implementation of an innovative system for monitoring the state of the sea in climate change scenarios" project, funded by the Interreg Italia-Malta Programme (https://iwavenet.eu/; notice 2/2019 Axis 3; project code C2-3.2-106) and the ARCHIMEDE "MultidisciplinARy approaCH to better define vulnerabIlity and hazard of MEDicanEs along the Ionian coasts of Sicily" project (code P2022MJKMA). We also thank

the grant PIACERI, 2020-22 programme: PAROSSISMA project (code 22722132140, principal investigator Marco Viccaro) and Open Access. A.M.B. thanks the PON "Ricerca e Innovazione 2014-2020 Azione IV.5 – Dottorati su tematiche green". The authors are grateful to Prof. Vittorio Scribano, the Museo Archeologico di Kamarina, Parco di Kamarina e Cava D'Ispica - Direttore Arch. Domenico Buzzone and the Centro Polifunzionale di Protezione Civile – Dott.ssa Emilia Pluchinotta, for hosting the seismic stations installed in the framework of the i-waveNET project and used in this work (IWAV2, IWAV3, IWAV3). This study has been conducted using E.U. Copernicus Marine Service Information, https://doi.org/10.25423/cmcc/medsea_multiyear_wav_006_012. The seismic data, downloaded using the EIDA and ORFEUS webservices, belong to the AC, FR, HC, HL, HP, IV, ML and MN networks. T.L. and R.D.P. thank the research project "SEISMOSTORM" funded by the BRAIN-be 2 program of the Federal Science Policy (BELSPO). We thank the handling editor Jiping Xie,and the anonymous reviewers for comments that helped clarify our paper.

References

- Agenzia per la Protezione dell'Ambiente e per i Servizi Tecnici Dipartimento Tutela Acque Interne e Marine Servizio Mareografico - Atlante delle onde nei mari italiani - Università degli studi di Roma Tre http://opac.apat.it/sebina/repository/catalogazione/immagini/pdf/atlante%20mari%201_60_2_.pdf
- Androulidakis, Y., Makris, C., Mallios, Z., Pytharoulis, I., Baltikas, V., & Krestenitis, Y. Storm surges during a Medicane in the Ionian Sea. *Proceedings of the Marine and Inland Waters Research Symposium, Porto Heli, Greece*. p. 16-19, 2022..

- Ardhuin, F., & Roland, A. "Coastal wave reflection, directional spread, and seismoacoustic noise sources." *Journal of Geophysical Research: Oceans* 117.C11, 2012.
- Ardhuin, F.; Gualtieri, L.; Stutzmann, E. How ocean waves rock the Earth: Two mechanisms explain microseisms with periods 3 to 300 s. *Geophysical Research Letters*, 42.3: 765-772, https://doi.org/10.1002/2014GL062782, 2015.
- Ardhuin, F., Stopa, J. E., Chapron, B., Collard, F., Husson, R., Jensen, R. E., ... & Young, I. Observing sea states. *Frontiers in Marine Science*, 124, https://doi.org/10.3389/fmars.2019.00124, 2019.
- Battaglia, J., & Aki, K. Location of seismic events and eruptive fissures on the Piton de la Fournaise volcano using seismic amplitudes. *Journal of Geophysical Research: Solid Earth*, *108*(B8), https://doi.org/10.1029/2002JB002193, 2003.
- Battaglia, J., Aki, K., & Ferrazzini, V. Location of tremor sources and estimation of lava output using tremor source amplitude on the Piton de la Fournaise volcano: 1. Location of tremor sources. Journal of volcanology and geothermal research, 147(3-4), 268-290, https://doi.org/10.1016/j.jvolgeores.2005.04.005, 2005.
- Bencivenga, M., Nardone, G., Ruggiero, F., & Calore, D., The Italian Data Buoy Network. *WTI Trans. Eng. Sci.*, 74, 321–332, 2012.
- Borzì, A. M., Minio, V., Cannavò, F., Cavallaro, A., D'Amico, S., Gauci, A., ... & Cannata, A. Monitoring extreme meteo-marine events in the Mediterranean area using the microseism (Medicane Apollo case study). *Scientific Reports*, *12*(1), 21363, https://doi.org/10.1038/s41598-022-25395-9, 2022.
- Bouin, M. N., & Lebeaupin Brossier, C. Surface processes in the 7 November 2014 medicane from air–sea coupled high-resolution numerical modelling. *Atmospheric Chemistry and Physics*, *20*(11), 6861-6881, 2020.

- Bromirski, Peter D., Reinhard E. Flick, and Nicholas Graham. "Ocean wave height determined from inland seismometer data: Implications for investigating wave climate changes in the NE Pacific." *Journal of Geophysical Research: Oceans* 104.C9 20753-20766, https://doi.org/10.1029/1999JC900156, 1999.
- Bromirski, Peter D. "Vibrations from the “perfect storm”." *Geochemistry, Geophysics, Geosystems* 2.7, https://doi.org/10.1029/2000GC000119, 2001.
- Bromirski, Peter D., Fred K. Duennebier, and Ralph A. Stephen. "Mid-ocean microseisms." *Geochemistry, Geophysics, Geosystems* 6.4, https://doi.org/10.1029/2004GC000768, 2005.
- Cannata, A., Di Grazia, G., Aliotta, M., Cassisi, C., Montalto, P., & Patanè, D. Monitoring seismo-volcanic and infrasonic signals at volcanoes: Mt. Etna case study. *Pure and Applied Geophysics*, *170*, 1751-1771, https://doi.org/10.1007/s00024-012-0634-x, 2013.
- Cannata, A., Cannavò, F., Moschella, S., Di Grazia, G., Nardone, G., Orasi, A., ... & Gresta, S. Unravelling the relationship between microseisms and spatial distribution of sea wave height by statistical and machine learning approaches. *Remote Sensing*, *12*(5), 761, https://doi.org/10.3390/rs12050761, 2020.
- Carrió, D. S., Homar, V., Jansa, A., Romero, R., & Picornell, M. A. Tropicalization process of the 7 November 2014 Mediterranean cyclone: Numerical sensitivity study. *Atmospheric Research*, *197*, 300-312, https://doi.org/10.1016/j.atmosres.2017.07.018, 2017.
- Capodici, F., Cosoli, S., Ciraolo, G., Nasello, C., Maltese, A., Poulain, P. M., ... & Gauci, A. Validation of HF radar sea surface currents in the Malta-Sicily Channel. *Remote sensing of environment*, *225*, 65-76, https://doi.org/10.1016/j.rse.2019.02.026, 2019.

- Cavicchia, Leone, Hans von Storch, and Silvio Gualdi. "Mediterranean tropical-like cyclones in present and future climate." *Journal of Climate* 27.19, 7493-7501, https://doi.org/10.1175/JCLI-D-14-00339.1, 2014.
- Comellas Prat, A., Federico, S., Torcasio, R. C., D'Adderio, L. P., Dietrich, S., & Panegrossi, G. Evaluation of the sensitivity of medicane Ianos to model microphysics and initial conditions using satellite measurements. *Remote Sensing*, *13*(24), 4984, https://doi.org/10.3390/rs13244984, 2021.
- Cutroneo, L., Ferretti, G., Barani, S., Scafidi, D., De Leo, F., Besio, G., & Capello, M.. Near real-time monitoring of significant sea wave height through microseism recordings: Analysis of an exceptional sea storm event. *Journal of Marine Science and Engineering*, *9*(3), 319, https://doi.org/10.3390/jmse9030319, 2021.
- D'Adderio, L. P., Panegrossi, G., Dafis, S., Rysman, J. F., Casella, D., Sanò, P., ... & Miglietta, M. M. Helios and Juliette: Two Falsely Acclaimed Medicanes. *Available at SSRN 4542818*.
- Dafis, S., Rysman, J. F., Claud, C., & Flaounas, E. Remote sensing of deep convection within a tropical-like cyclone over the Mediterranean Sea. *Atmospheric Science Letters*, *19*(6), e823, https://doi.org/10.1002/asl.823, 2018.
- Davies R. Cyclone Helios, Malta and Italy, February 2023, https://www.efas.eu/en/news/cyclone-helios-malta-and-italy-february-2023, last access 13/04/2023)
- Delibera di Giunta - Regione Siciliana (https://www2.regione.sicilia.it/deliberegiunta/file/giunta/allegati/N.099_15.02.2023.pdf, last access 13/04/2023)
- Di Muzio, E., Riemer, M., Fink, A. H., & Maier-Gerber, M. Assessing the predictability of Medicanes in ECMWF ensemble forecasts using an object-based approach.

Formatted: Font: (Default) Times New Roman, 12 pt

Formatted: Font: (Default) Times New Roman, 12 pt, English (United States)

Formatted: Font: (Default) Times New Roman, 12 pt

Quarterly Journal of the Royal Meteorological Society, *145*(720), 1202-1217, https://doi.org/10.1002/qj.3489, 2019.

- Emanuel, K. Increasing destructiveness of tropical cyclones over the past 30 years. *Nature*, *436*(7051), 686-688, https://doi.org/10.1038/nature03906, 2005.
- Faranda, D., Bourdin, S., Ginesta, M., Krouma, M., Noyelle, R., Pons, F., ... & Messori, G. A climate-change attribution retrospective of some impactful weather extremes of 2021. *Weather and Climate Dynamics*, *3*(4), 1311-1340, https://doi.org/10.5194/wcd-3-1311-2022, 2022.
- Ferretti, G., Zunino, A., Scafidi, D., Barani, S., & Spallarossa, D. On microseisms recorded near the Ligurian coast (Italy) and their relationship with sea wave height. *Geophysical Journal International*, *194*(1), 524-533, https://doi.org/10.1093/gji/ggt114, 2013.
- Ferretti, G., Barani, S., Scafidi, D., Capello, M., Cutroneo, L., Vagge, G., & Besio, G. Near real-time monitoring of significant sea wave height through microseism recordings: An application in the Ligurian Sea (Italy). *Ocean & Coastal Management*, *165*, 185-194, https://doi.org/10.3390/jmse9030319, 2018.
- Flaounas, E., Davolio, S., Raveh-Rubin, S., Pantillon, F., Miglietta, M. M., Gaertner, M. A., ... & Ricard, D. Mediterranean cyclones: Current knowledge and open questions on dynamics, prediction, climatology and impacts. *Weather and Climate Dynamics*, *3*(1), 173-208, https://doi.org/10.5194/wcd-3-173-2022, 2022.
- Gerstoft, P., Fehler, M. C., & Sabra, K. G. When katrina hit california. *Geophysical Research Letters*, *33*(17), https://doi.org/10.1029/2006GL027270, 2006.
- Gualtieri, L., Camargo, S. J., Pascale, S., Pons, F. M., & Ekström, G. The persistent signature of tropical cyclones in ambient seismic noise. *Earth and Planetary Science Letters*, *484*, 287-294, https://doi.org/10.1016/j.epsl.2017.12.026, 2018.

- Guerin, G., Rivet, D., Van Den Ende, M. P. A., Stutzmann, E., Sladen, A., & Ampuero, J. P. Quantifying microseismic noise generation from coastal reflection of gravity waves recorded by seafloor DAS. *Geophysical Journal International*, *231*(1), 394-407, https://doi.org/10.1093/gji/ggac200, 2022.
- Johnson, R. W. (2001). An introduction to the bootstrap. Teaching statistics, 23(2), 49-54.
- Hart, R. E. A cyclone phase space derived from thermal wind and thermal asymmetry. *Monthly weather review*, *131*(4), 585-616, https://doi.org/10.1175/1520-0493(2003)131%3C0585:ACPSDF%3E2.0.CO;2, 2003.
- Hasselmann, Klaus. "A statistical analysis of the generation of microseisms." *Reviews of Geophysics* 1.2, 177-210, 1963.
- Haubrich, Richard A., and Keith McCamy. "Microseisms: Coastal and pelagic sources." *Reviews of Geophysics* 7.3: 539-571, 1969.
- Kerkmann J. and Bachmeier S. Development of a tropical storm in the Mediterranean Sea (6–9 November 2011). Available at: https://www.eumetsat.int/tropical-storm-develops-mediterranean-sea (last access: 15 February 2023), 2011.
- Korres, G., Ravdas, M., & Zacharioudaki, A. Mediterranean Sea Waves Hindcast (CMEMS MED-Waves) [Data set]. Copernicus Monitoring Environment Marine Service (CMEMS). https://doi.org/10.25423/CMCC/MEDSEA_HINDCAST_WAV_006_012, 2019
- Kumagai, H., Placios, P., Ruiz, M., Yepes, H., & Kozono, T. Ascending seismic source during an explosive eruption at Tungurahua volcano, Ecuador. *Geophysical Research Letters*, *38*(1), https://doi.org/10.1029/2010GL045944, 2011.

- Lagouvardos, K., Karagiannidis, A., Dafis, S., Kalimeris, A., & Kotroni, V. Ianos—A hurricane in the Mediterranean. *Bulletin of the American Meteorological Society*, *103*(6), E1621-E1636, https://doi.org/10.1175/BAMS-D-20-0274.1, 2022.
- Lepore,S and Grad, M. "Analysis of the primary and secondary microseisms in the wavefield of the ambient noise recorded in northern Poland." *Acta Geophysica*: 66, 915-929 , 2018.
- Lin, J., Lin, J., & Xu, M. Microseisms generated by super typhoon Megi in the western Pacific Ocean. *Journal of Geophysical Research: Oceans*, *122*(12), 9518-9529, https://doi.org/10.1002/2017JC013310, 2017.
- Lionello, P., Conte, D., & Reale, M. The effect of cyclones crossing the Mediterranean region on sea level anomalies on the Mediterranean Sea coast. *Natural Hazards and Earth System Sciences*, *19*(7), 1541-1564, https://doi.org/10.5194/nhess-19-1541-2019, 2019.
- Long, R. M., Barrick, D., Largier, J. L., & Garfield, N. Wave observations from central California: SeaSonde systems and in situ wave buoys. *Journal of Sensors*, https://doi.org/10.1155/2011/728936, *2011*.
- Longuet-Higgins, Michael Selwyn. "A theory of the origin of microseisms." *Philosophical Transactions of the Royal Society of London. Series A, Mathematical and Physical Sciences* 243.857, 1-35, 1950.
- Lorente, P., Lin-Ye, J., Garcia-Leon, M., Reyes, E., Fernandes, M., Sotillo, M. G., ... & Alvarez-Fanjul, E. On the performance of high frequency radar in the western mediterranean during the record-breaking storm gloria. *Frontiers in Marine Science*, *8*, 645762, https://doi.org/10.3389/fmars.2021.645762, 2021.
- Miglietta, M. M., Moscatello, A., Conte, D., Mannarini, G., Lacorata, G., & Rotunno, R. Numerical analysis of a Mediterranean 'hurricane'over south-eastern Italy:

Formatted: Font: (Default) Times New Roman, 12 pt

Sensitivity experiments to sea surface temperature. *Atmospheric research*, *101*(1-2), 412-426, https://doi.org/10.1016/j.atmosres.2011.04.006, 2011.

- Miglietta, M. M., Laviola, S., Malvaldi, A., Conte, D., Levizzani, V., & Price, C. Analysis of tropical-like cyclones over the Mediterranean Sea through a combined modeling and satellite approach. *Geophysical Research Letters*, *40*(10), 2400-2405, https://doi.org/10.1002/grl.50432, 2013.
- Miglietta, M. M., & Rotunno, R. Development mechanisms for Mediterranean tropical-like cyclones (medicanes). *Quarterly Journal of the Royal Meteorological Society*, *145*(721), 1444-1460, https://doi.org/10.1002/qj.3503, 2019.
- Moschella, S., Cannata, A., Cannavò, F., Di Grazia, G., Nardone, G., Orasi, A., ... & Gresta, S. Insights into microseism sources by array and machine learning techniques: Ionian and Tyrrhenian sea case of study. *Frontiers in Earth Science*, *8*, 114, https://doi.org/10.3389/feart.2020.00114, 2020.
- Nastos, P. T., Papadimou, K. K., & Matsangouras, I. T. Mediterranean tropical-like cyclones: Impacts and composite daily means and anomalies of synoptic patterns. *Atmospheric Research*, *208*, 156-166, https://doi.org/10.1016/j.atmosres.2017.10.023, 2018.
- Oliver, J., & Page, R. Concurrent storms of long and ultralong period microseisms. *Bulletin of the Seismological Society of America*, *53*(1), 15-26, 1963.
- Orasi, A., Picone, M., Drago, A., Capodici, F., Gauci, A., Nardone, G., ... & Alonso-Martirena, A. HF radar for wind waves measurements in the Malta-Sicily Channel. *Measurement*, *128*, 446-454, https://doi.org/10.1016/j.measurement.2018.06.060, 2018.
- Pravia-Sarabia, E., Gómez-Navarro, J. J., Jiménez-Guerrero, P., & Montávez, J. P. Influence of sea salt aerosols on the development of Mediterranean tropical-like

911 cyclones. *Atmospheric Chemistry and Physics*, *21*(17), 13353-13368,
912 https://doi.org/10.5194/acp-21-13353-2021, 2021.
913 ● Portmann, R., González-Alemán, J. J., Sprenger, M., & Wernli, H. How an uncertain
914 short-wave perturbation on the North Atlantic wave guide affects the forecast of an
915 intense Mediterranean cyclone (Medicane Zorbas). *Weather and Climate Dynamics*,
916 *1*(2), 597-615, https://doi.org/10.5194/wcd-1-597-2020, 2020.
917 ● Reguero, B. G., Losada, I. J., & Méndez, F. J. A recent increase in global wave power
918 as a consequence of oceanic warming. *Nature communications*, *10*(1), 205,
919 https://doi.org/10.1038/s41467-018-08066-0, 2019.
920 ● Retailleau, L., & Gualtieri, L. Toward high-resolution period-dependent seismic
921 monitoring of tropical cyclones. *Geophysical Research Letters*, *46*(3), 1329-1337,
922 https://doi.org/10.1029/2018GL080785, 2019.
923 ● Retailleau, L., & Gualtieri, L. Multi-phase seismic source imprint of tropical cyclones.
924 *Nature communications*, *12*(1), 2064, https://doi.org/10.1038/s41467-021-22231-y,
925 2021.
926 ● Rost, S., & Thomas, C. Array seismology: Methods and applications. *Reviews of*
927 *geophysics*, *40*(3), 2-1, https://doi.org/10.1029/2000RG000100, 2002.
928 ● Rumora, I., Jukić, O., Filić, M., & Filjar, R. A study of GPS positioning error associated
929 with tropospheric delay during Numa Mediterranean cyclone. *Int J for Transp and Traff*
930 *Eng*, *8*(3), 282-293, https://doi.org/10.7708/ijtte.2018.8(3).03, 2018.
931 ● Sarpkaya, T., & Isaacson, M. Mechanics of wave forces on offshore structures Van
932 Nostrand Reinhold Company New York. *New York*, 1981.
933 ● Saviano, S., Kalampokis, A., Zambianchi, E., & Uttieri, M. A year-long assessment of
934 wave measurements retrieved from an HF radar network in the Gulf of Naples

(Tyrrhenian Sea, Western Mediterranean Sea). *Journal of Operational Oceanography*, *12*(1), 1-15, https://doi.org/10.1080/1755876X.2019.1565853, 2019.

- Scardino, G., Scicchitano, G., Chirivì M., Costa P.J.M., Luparelli A., Mastronuzzi G. Convolutional Neural Network and Optical Flow for the Assessment ofWave and Tide Parameters from Video Analysis (LEUCOTEA): An Innovative Tool for Coastal Monitoring. Remote Sensing, 14, 2994, doi.org/10.3390/rs14132994, 2022.
- Scicchitano, G., Scardino, G., Monaco, C., Piscitelli, A., Milella, M., De Giosa, F., & Mastronuzzi, G. Comparing impact effects of common storms and Medicanes along the coast of south-eastern Sicily. *Marine Geology*, *439*, 106556, https://doi.org/10.1016/j.margeo.2021.106556, 2021.
- Shaltout, M., & Omstedt, A. Recent sea surface temperature trends and future scenarios for the Mediterranean Sea. *Oceanologia*, *56*(3), 411-443, https://doi.org/10.5697/oc.56-3.411, 2014.
- Soubestre, J., Shapiro, N. M., Seydoux, L., de Rosny, J., Droznin, D. V., Droznina, S. Y., ... & Gordeev, E. I. Network-based detection and classification of seismovolcanic tremors: Example from the Klyuchevskoy volcanic group in Kamchatka. *Journal of Geophysical Research: Solid Earth*, *123*(1), 564-582, https://doi.org/10.1002/2017JB014726, 2018.
- Sun, T., Xue, M., Le, K. P., Zhang, Y., & Xu, H. Signatures of ocean storms on seismic records in South China Sea and East China Sea. *Marine Geophysical Research*, *34*, 431-448, https://doi.org/10.1007/s11001-013-9204-6, 2013.
- Tous, M., & Romero, R. Meteorological environments associated with medicane development. *International Journal of Climatology*, *33*(1), 1-14, https://doi.org/10.1002/joc.3428, 2013.

- Trnkoczy, A., Bormann, P., Hanka, W., Holcomb, L. G., Nigbor, R. L., Shinohara, M., ... & Suyehiro, K. Site selection, preparation and installation of seismic stations. In *New Manual of Seismological Observatory Practice 2 (NMSOP-2)* (pp. 1-139). Deutsches GeoForschungsZentrum GFZ, 2012.
- Tweet medcyclones: https://twitter.com/medcyclones/status/1623795373423620096?s=20, https://twitter.com/medcyclones/status/1623992335104081921?s=20, https://twitter.com/medcyclones/status/1624143740800536591?s=20
- Varlas, G., Vervatis, V., Spyrou, C., Papadopoulou, E., Papadopoulos, A., & Katsafados, P. Investigating the impact of atmosphere–wave–ocean interactions on a Mediterranean tropical-like cyclone. *Ocean Modelling*, *153*, 101675, https://doi.org/10.1016/j.ocemod.2020.101675, 2020.
- Welch, P. D. The use of Fast Fourier Transform for the estimation of power spectra: a method based on time averaging over short, modified periodograms, IEEE T. Audio Electroacoust. 15, 70–73, https://doi.org/10.1109/TAU.1967.1161901, 1967.
- Zhang, J., Gerstoft, P., & Bromirski, P. D. Pelagic and coastal sources of P-wave microseisms: Generation under tropical cyclones. *Geophysical Research Letters*, *37*(15), https://doi.org/10.1029/2010GL044288, 2010.
- Zimbo, F., Ingemi, D., & Guidi, G. The tropical-like cyclone “ianos” in September 2020. *Meteorology*, *1*(1), 29-44, https://doi.org/10.3390/meteorology1010004, 2022.

Formatted: Indent: Left: 0,63 cm, No bullets or numbering

Authors Contribution

A.M.B., A.C. and F.C. conceived the idea. A.M.B. analyzed seismic data and V.M. performed array analysis. C.L.R, G.N., A.O. and M.P. analyzed buoys data. S.A., D.C., G.D.G., G.L., S.D., R.D. and T.L. helped perform seismic analysis. F.C., G.C., S.A., I.F., G.G. G.M., analyzed HF Radar Data. A.M.B. and V.M. wrote the paper. S.A., F.C., D.C., G.L. and V.M. dealt with the new seismic installation. G.C. lead one of the projects funding this research, G.S. helped to interpret the sea state data. All the authors discussed the results, edited the paper and gave consent for this publication under the supervision of A.C.

Figures

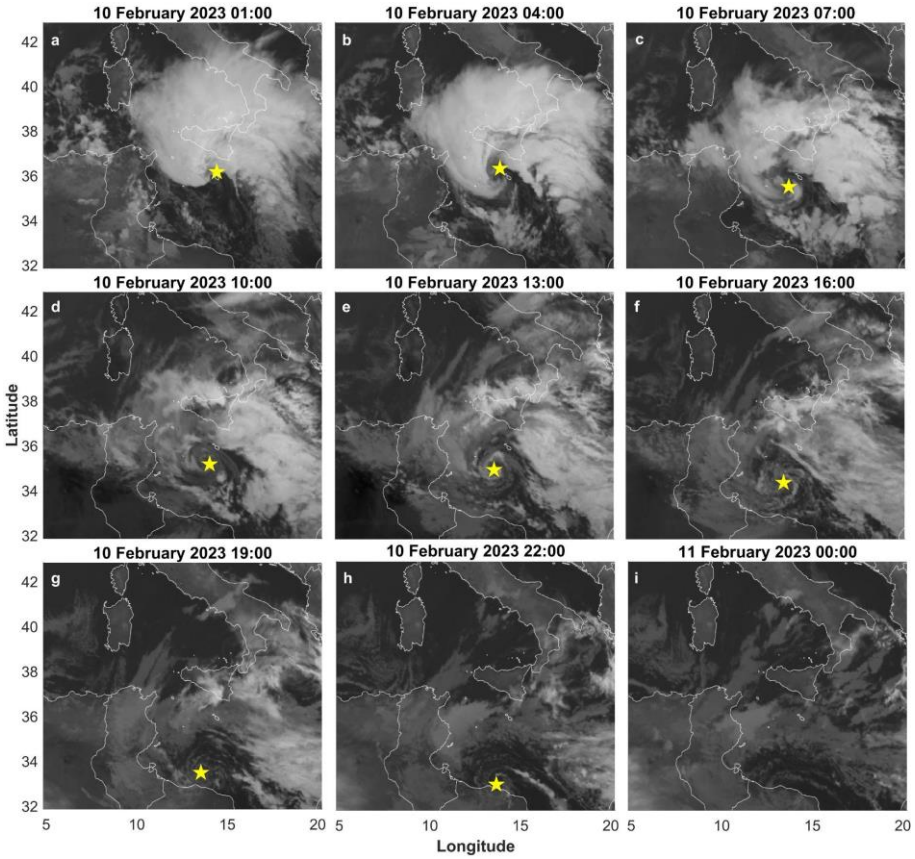

Figure 1: Satellite images of the Mediterranean area and of the sub-tropical system Helios during the period 10/02/2023 01:00 - 11/02/2023 00:00. The yellow stars in (a-h) show the position of the cyclone eye. The lack of the star in (i) is due to the dissipation of Helios after the landfall against the Libyan coast (h). (©EUMETSAT SEVIRI Images)

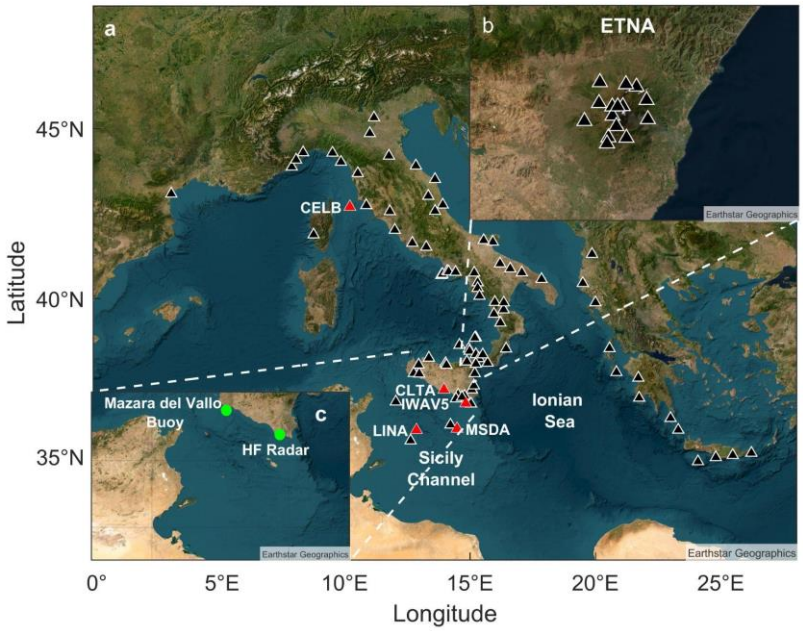

Figure 2: Satellite image of the Mediterranean area with a selection of the broadband seismic stations available in the ORFEUS and INGV databases and used in the spectral analysis and in the grid search method (a) and selection of the broadband seismic stations in the Etna area maintained by INGV-OE (b), used in the array analysis (base image source ©Earthstar Geographic). The red triangles indicate the stations used in the detailed analysis shown in Figures **3** and **9** and in **Supplementary Figures 1** and **2**. The green dots in (c) indicate the position of the wavemeter buoy (Mazara del Vallo) and of the HF Radar (Marina di Ragusa) used for the sea state monitoring.

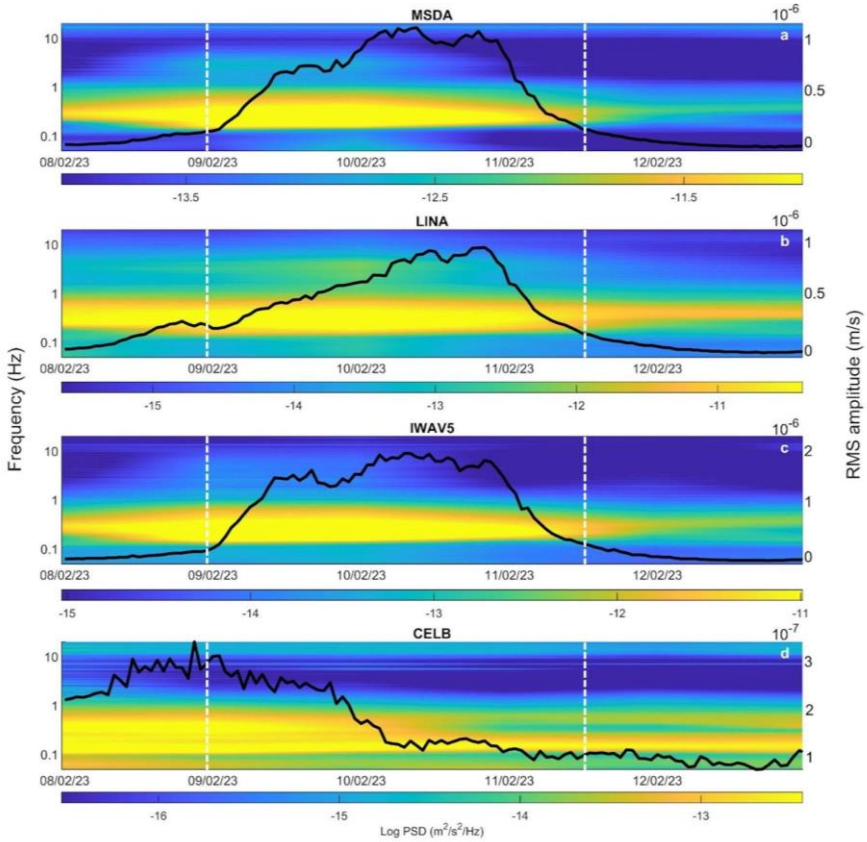

Figure 3: Spectrograms and RMS amplitude time series (black lines) for the SM band (0.1-0.2 Hz) of the seismic signal recorded by the vertical component of 4 stations located along the Maltese coastline (a), in Linosa Island (b), in the southern part of Sicily (c) and in Central Italy (d) (see **Figure 2a** for the station locations).

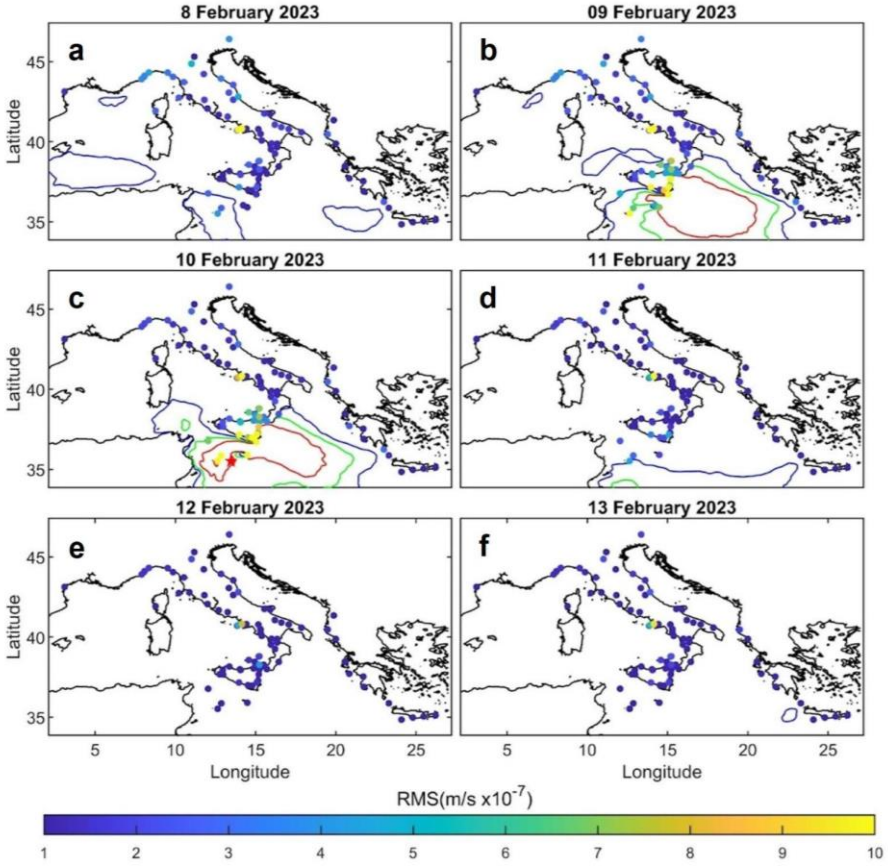

Figure 4: Spatial and temporal distribution of the RMS amplitude for the SM band computed at the 105 stations considered (dots). The colors of dots represent the RMS amplitude as specified in the color bar. The blue, green and red contour lines represent significant wave heights of 3, 4 and 5 m, respectively, while the red five-point star in (c) indicates the eye position of the sub-tropical system Helios obtained from satellite images.

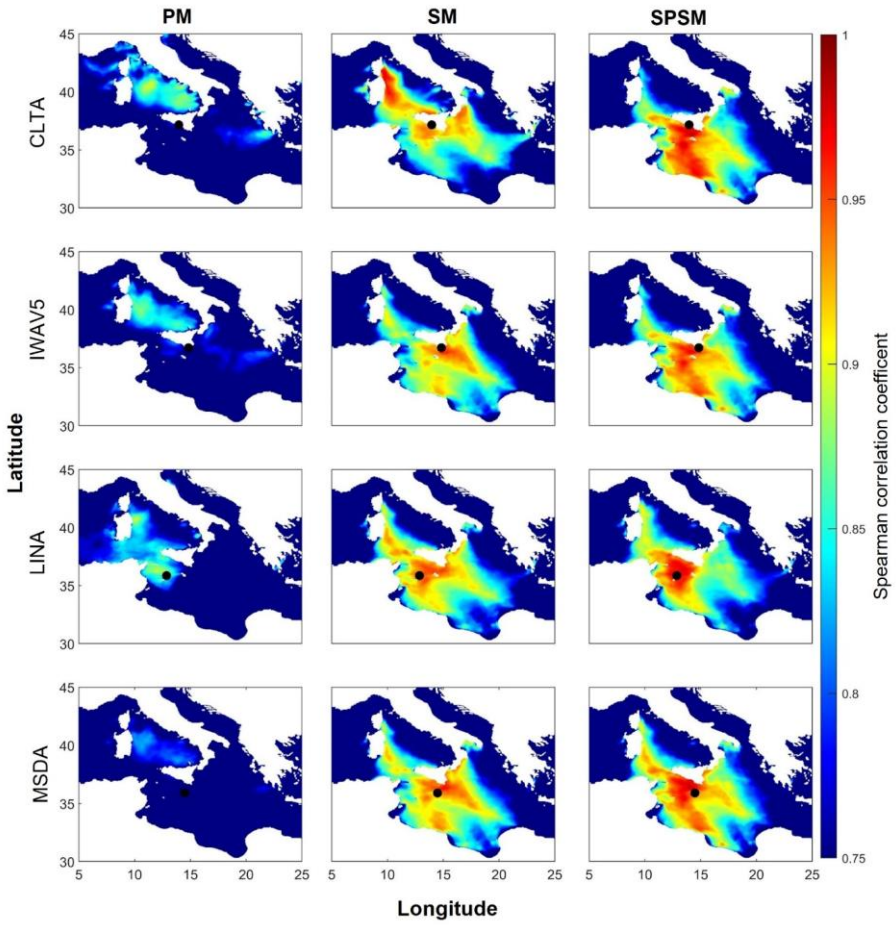

Figure 5: ….Correlation maps obtained for the vertical component of the seismic stations MSDA, LINA, CLTA and IWAV5 for the PM, SM and SPSM frequency bands during the period under investigation. The black dots indicates the position of the seismic station.

Formatted: Justified

Formatted: Left

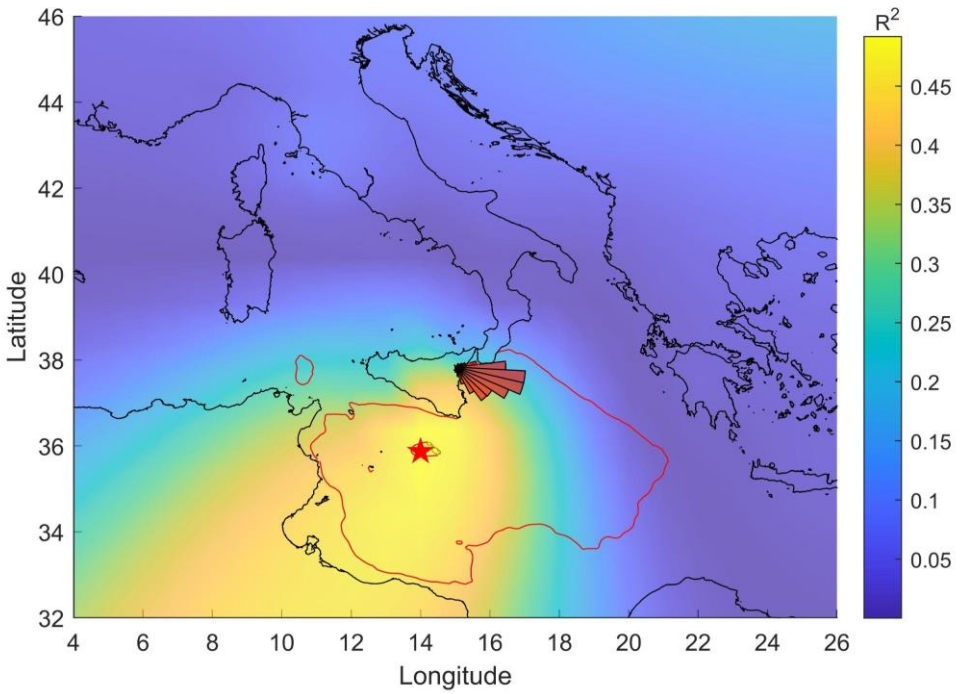

Figure ~~5~~6: Localization of the microseism source for 10 February 2023 at 16:00. The red five-point star indicates the centroid position of all the grid nodes whose R^2 values do not differ by more than 1% from the maximum R^2 value obtained with the grid search method, while the rose diagram, located at the center of the summit area of Mt. Etna (see **Figure 2b**), shows the distribution of the back azimuth values on the same day. The red contour line represents significant wave heights of 4 m obtained from the Copernicus product MEDSEA_HINDCAST_WAV_006_012 during the same time interval.

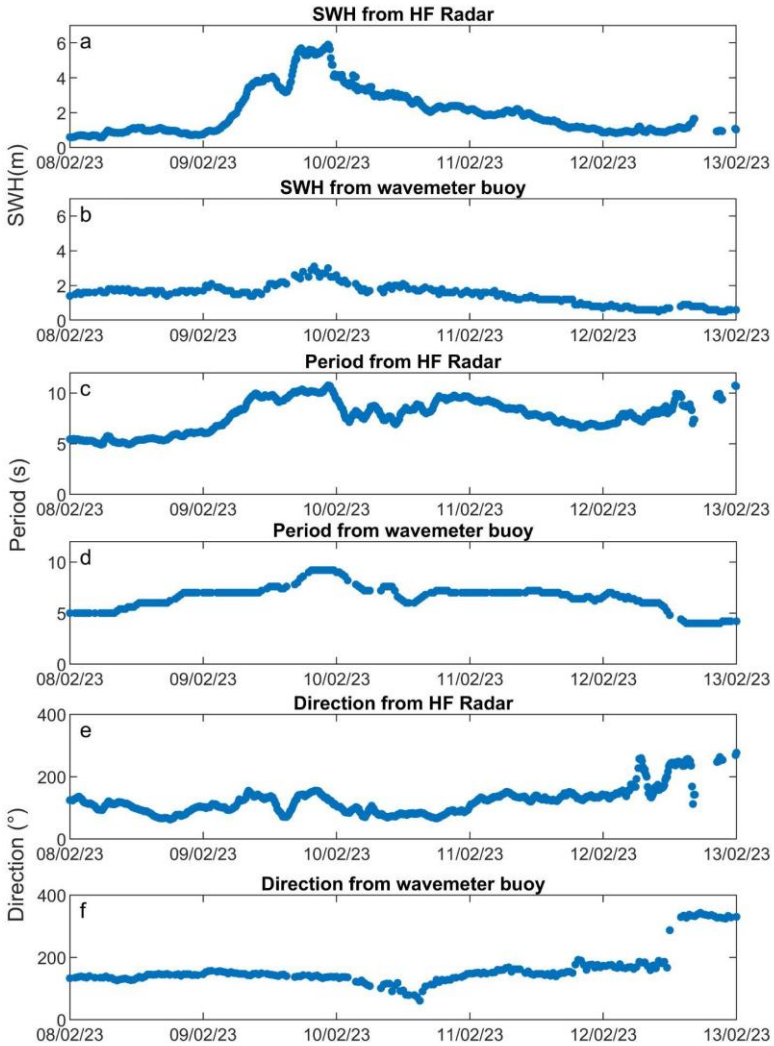

Figure 67: Wave features in terms of SWH, period and mean direction time series retrieved by using the HF Radar (a, c and e) and Mazara del Vallo buoy (b, d and f) data. For the instruments location see **Figure 2c.**

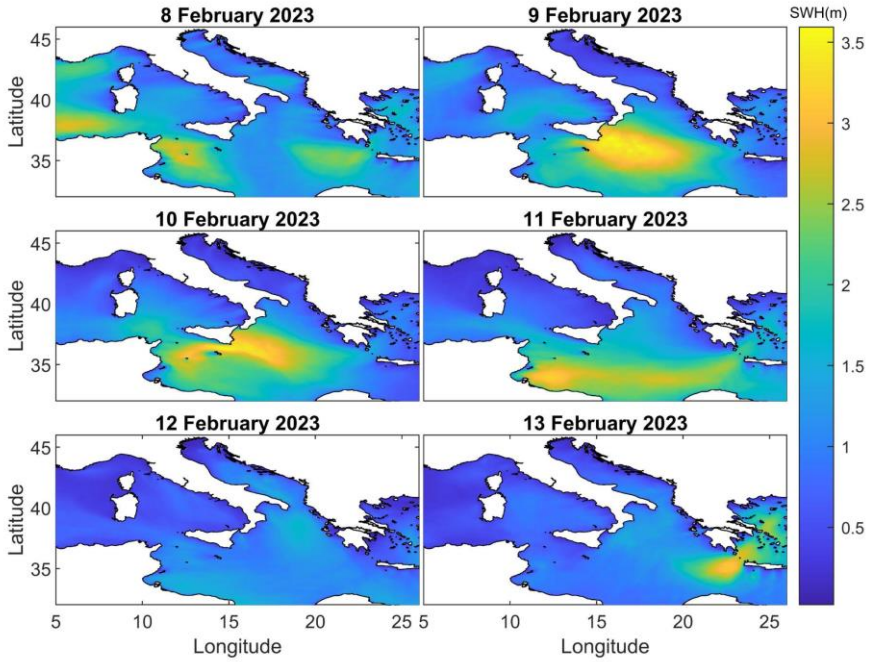

Figure ~~7~~8: Hindcast maps, obtained from the Copernicus product MEDSEA_HINDCAST_WAV_006_012, showing the spatio-temporal variations of SWH during the days taken into account.

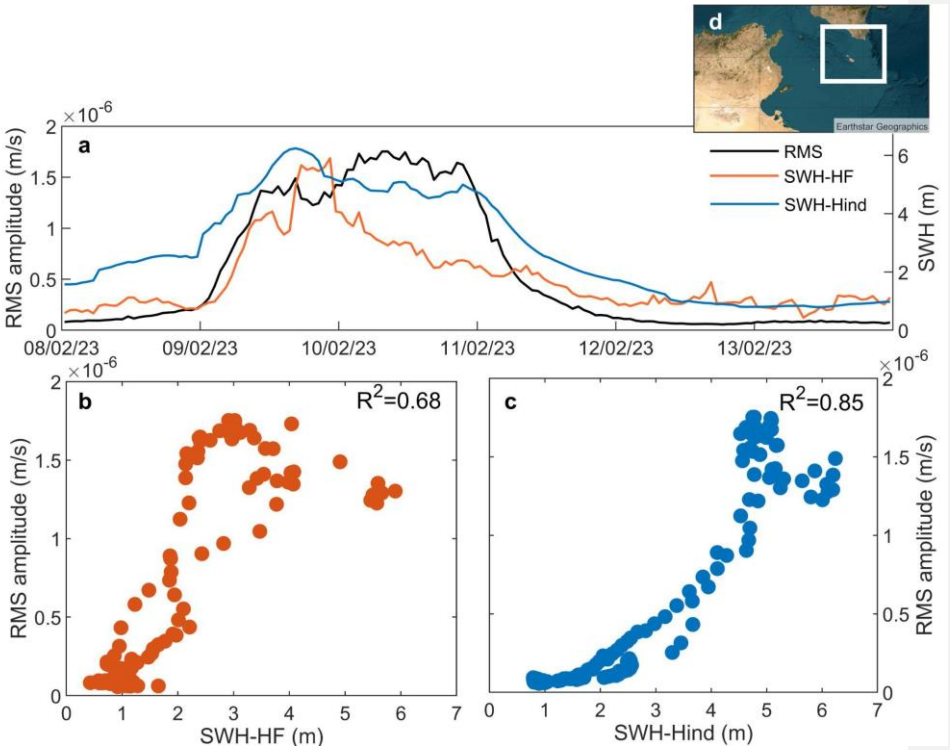

Figure 89: (a) RMS amplitude time series, recorded at the station IWAV5, and SWH time series retrieved by HF Radar (SWH-HF; orange line) and by hindcast data (SWH-Hind; light-blue). Cross-plot showing the relation between SWH-HF and RMS amplitude (b) and between SWH-Hind and RMS amplitude (c). The value of the determination coefficient (R^2) is reported in the upper right corner of the plots (b) and (c). In (d) the area of the Sicily Channel used to calculate the SWH-Hind time series is shown (base image source ©Earthstar Geographic). For the instruments location see **Figure 2a** and **2c**.

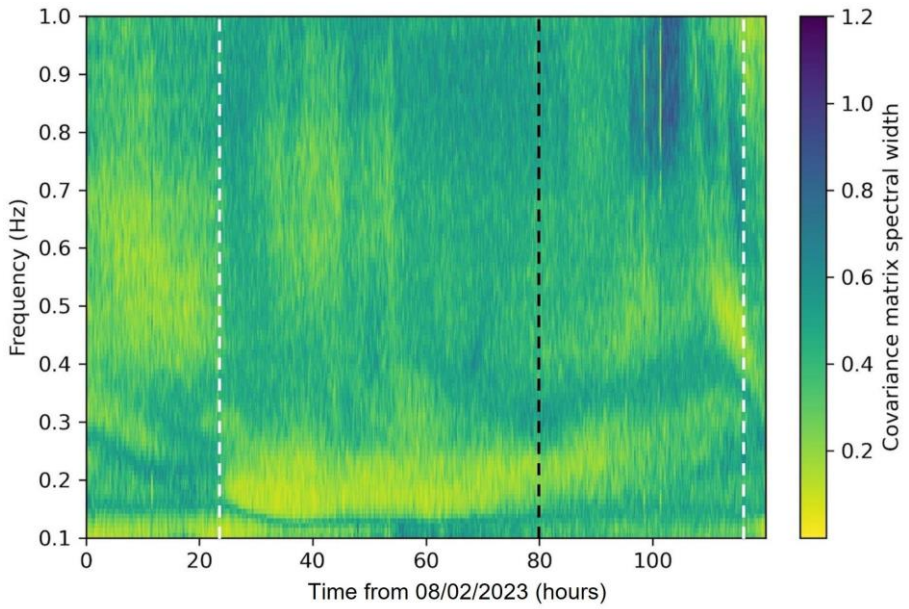

Figure ~~9~~10: Covariance matrix spectral width obtained for the period 8-12 February 2023 using the stations IWAV5, LINA, MSDA and CLTA. The white dashed lines represent the development and the ending of the sub-tropical system Helios, while the black dashed line indicates the time when Helios makes landfall against the Libyan coast. For stations location see **Figure 2a.**

1069 **Table**

Date	Hour	Longitude of microseism source (degrees)	Latitude of microseism source (degrees)	R^2 Value	Errors latitude (~~K~~km)	Errors longitude (~~K~~km)	Longitude of cyclone eye from satellite data (degrees)	Latitude cyclone from satellite data (degrees)
09/02/2023	08:00	15.0000	37.3681	0.3233	243	535	/	/
09/02/2023	12:00	15.0000	36.3681	0.3459	217	412	/	/
09/02/2023	16:00	15.0000	36.3681	0.3554	181	364	/	/
09/02/2023	20:00	15.0000	36.3681	0.3865	173	339	/	/
10/02/2023	00:00	14.5000	36.3681	0.4725	185	298	/	/
10/02/2023	04:00	14.5000	36.3681	0.5066	166	214	14.01584	36.24165
10/02/2023	08:00	14.3030	36.0348	0.5107	178	228	13.79612	35.57149
10/02/2023	12:00	14.3030	36.0348	0.5091	170	211	13.91697	35.13203
10/02/2023	16:00	14.0000	35.8681	0.4920	165	228	13.59836	34.5937
10/02/2023	20:00	14.0000	35.8681	0.4762	165	245	13.52146	33.59395
11/02/2023	00:00	14.0000	35.8681	0.3864	206	321	13.74118	32.9897

Formatted: Centered
Formatted Table
Formatted: Font: Bold
Formatted: Font: Bold
Formatted: Centered
Formatted: Font: Bold
Formatted: Font: Bold
Formatted: Centered
Formatted: Font: Bold
Formatted: Centered
Formatted: Font: Bold
Formatted: Centered
Formatted: Font: Bold
Formatted: Centered
Formatted: Font: Bold
Formatted: Centered

Table 1. Main features of the microseism sources and comparison with the coordinates of the cyclone eye retrieved from satellite data. The coordinates of the cyclone eye between 8:00 of 9 Febreuary and 00:00 of 10 February are absent since the cyclone eye is clearly visible between 01:00 and 23:00 of 10 February 2023.

Supplementary figures

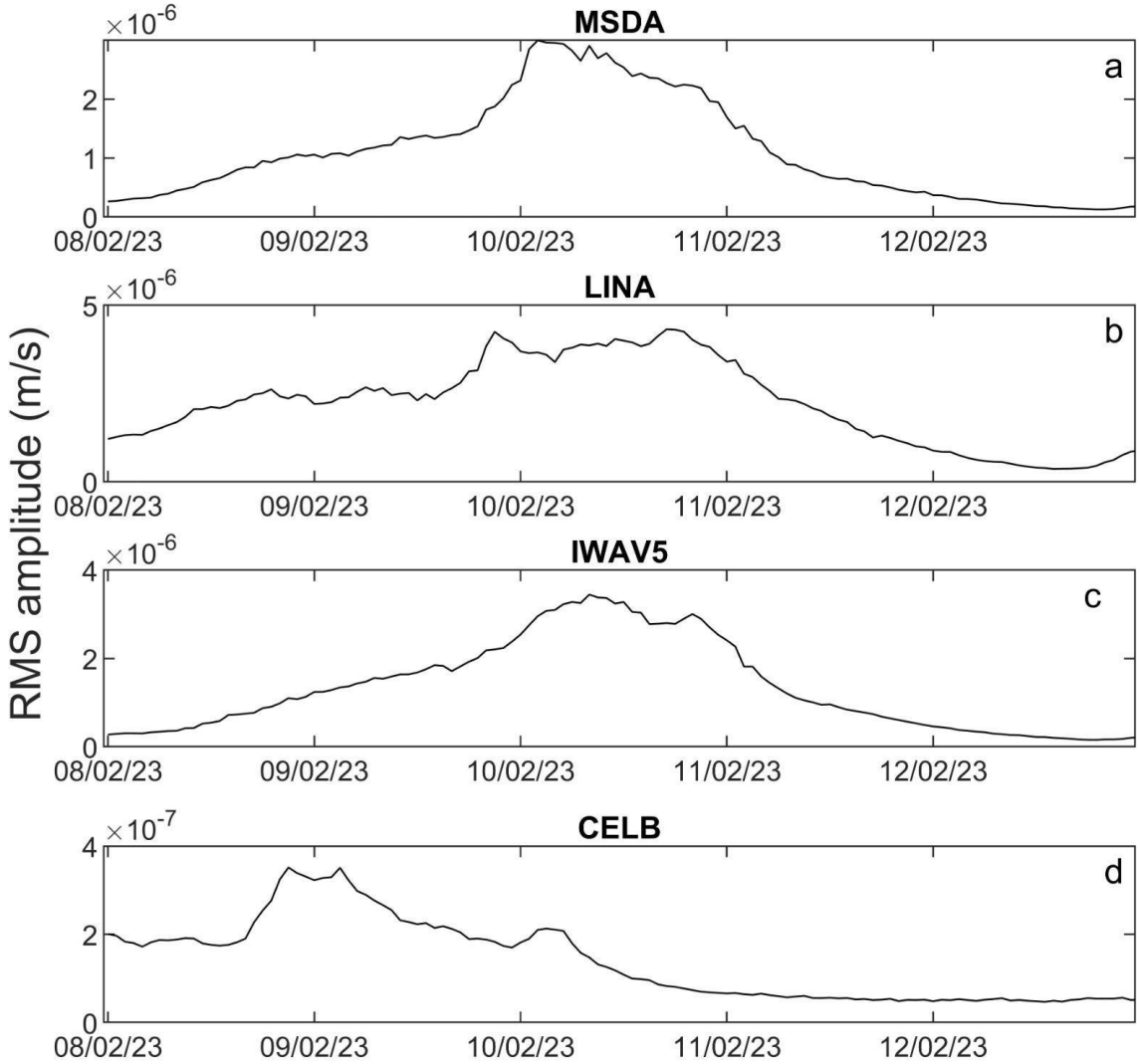

Supplementary Figure 1: RMS amplitude time series, for the SPSM band (0.2-0.4 Hz), of the seismic signal recorded by the vertical component of 4 stations located along the Maltese coastline (a), in Linosa Island (b), in the southern part of Sicily (c) and in Central Italy (d) (see **Figure 2a** for the station locations).

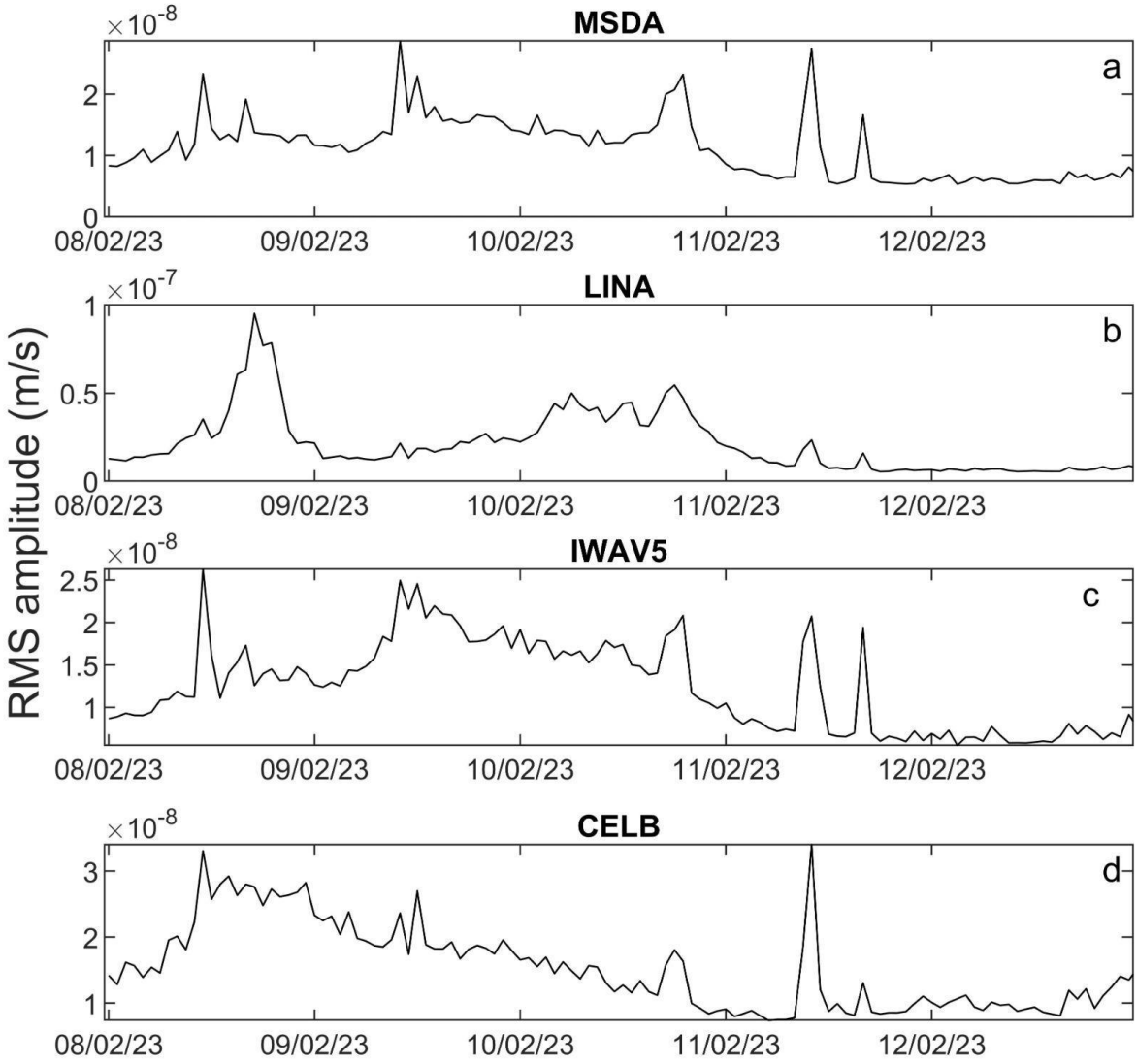

Supplementary Figure 2: RMS amplitude time series, for the PM band (0.05-0.07 Hz), of the seismic signal recorded by the vertical component of 4 stations located along the Maltese coastline (a), in Linosa Island (b), in the southern part of Sicily (c) and in Central Italy (d) (see **Figure 2a** for the station locations).

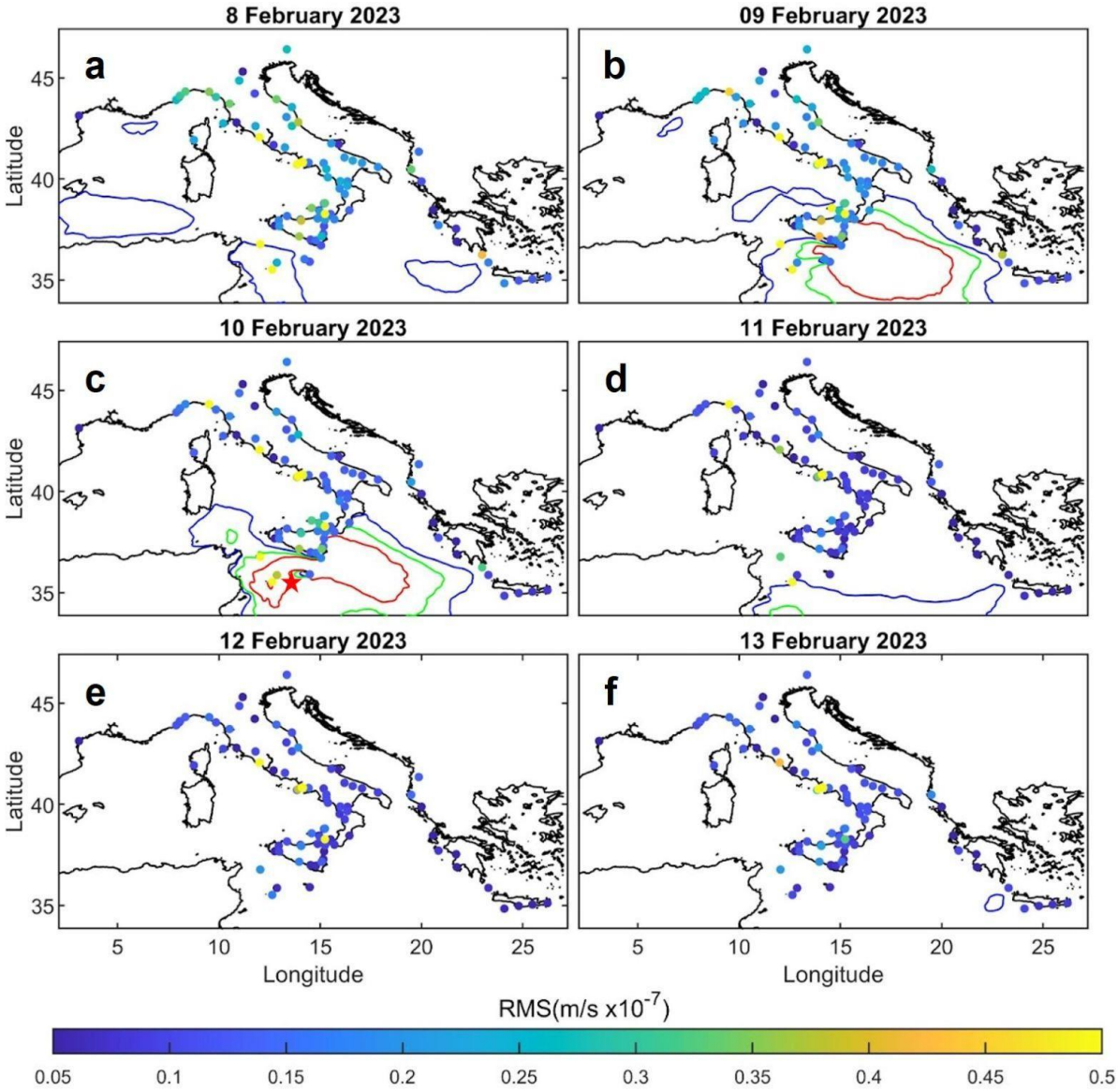

Supplementary Figure 3: Spatial and temporal distribution of the RMS amplitude for the PM band computed at 105 stations considered (dots). The colors of dots represent the RMS amplitude as specified in the color bar. The blue, green and red contour lines represent significant wave heights of 3, 4 and 5 m, respectively, while the red five-point star in (c) indicates the eye position of the sub-tropical system Helios obtained from satellite images.

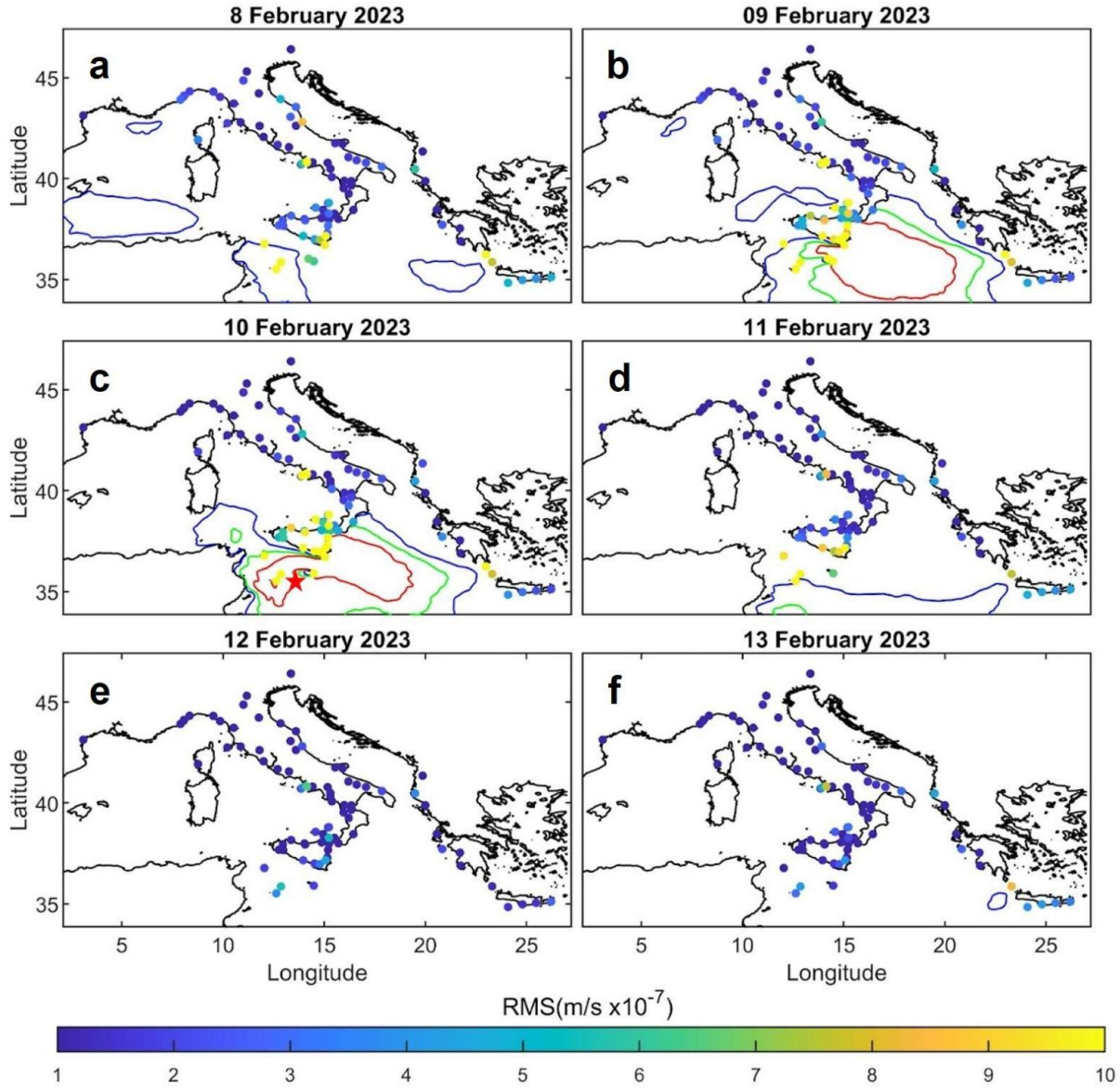

Supplementary figure 4: Spatial and temporal distribution of the RMS amplitude for the SPSM band computed at 105 stations considered (dots). The colors of dots represent the RMS amplitude as specified in the color bar. The blue, green and red contour lines represent significant wave heights of 3, 4 and 5 m, respectively, while the red five-point star in (c) indicates the eye position of the sub-tropical system Helios obtained from satellite images.

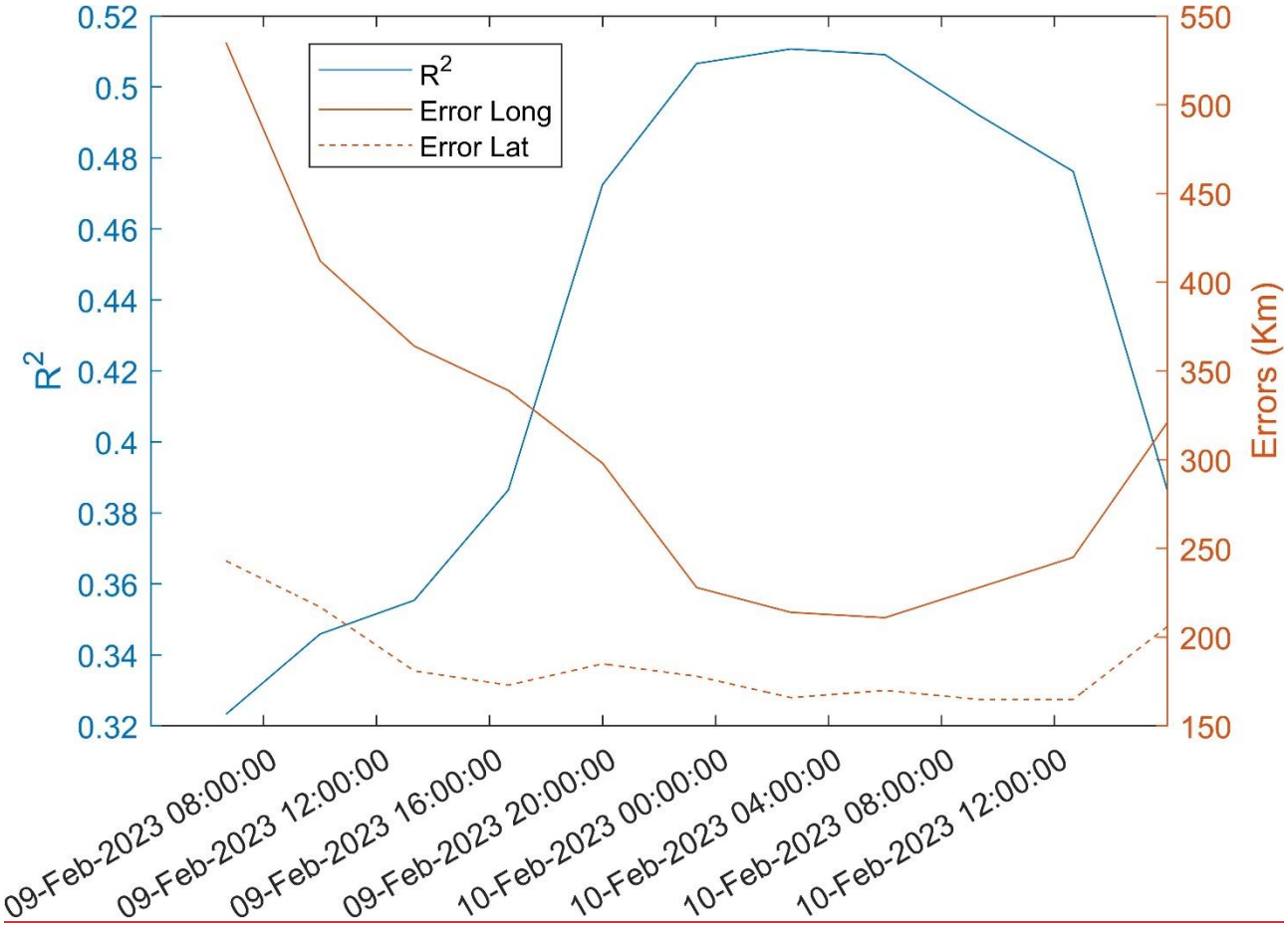

Supplementary Figure 5: Plot showing the inversely proportional relationship between the errors (orange lines) and the R^2 (blue line).

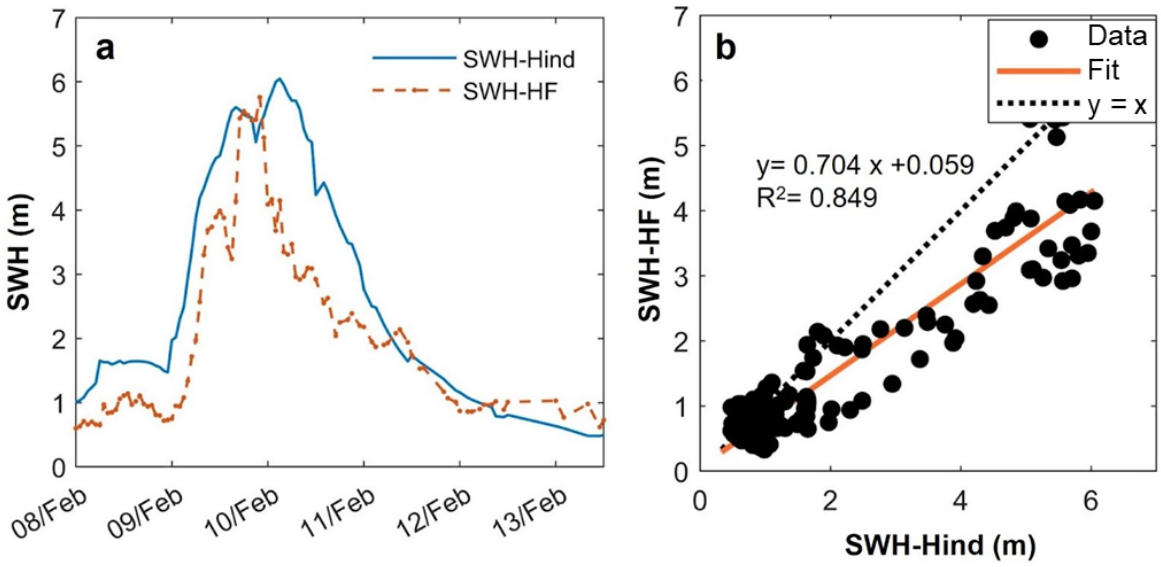

Supplementary Figure ~~5~~6: (a) Comparison between the SWH time series retrieved from hindcast data (SWH-Hind; light-blue line) and from HF Radar data (SWH-HF; orange dashed line). (b) Crossplot showing the agreement between SWH-Hind and SWH-HF data with a R^2 of 0.849. For the HF Radar location see **Figure 2c.**

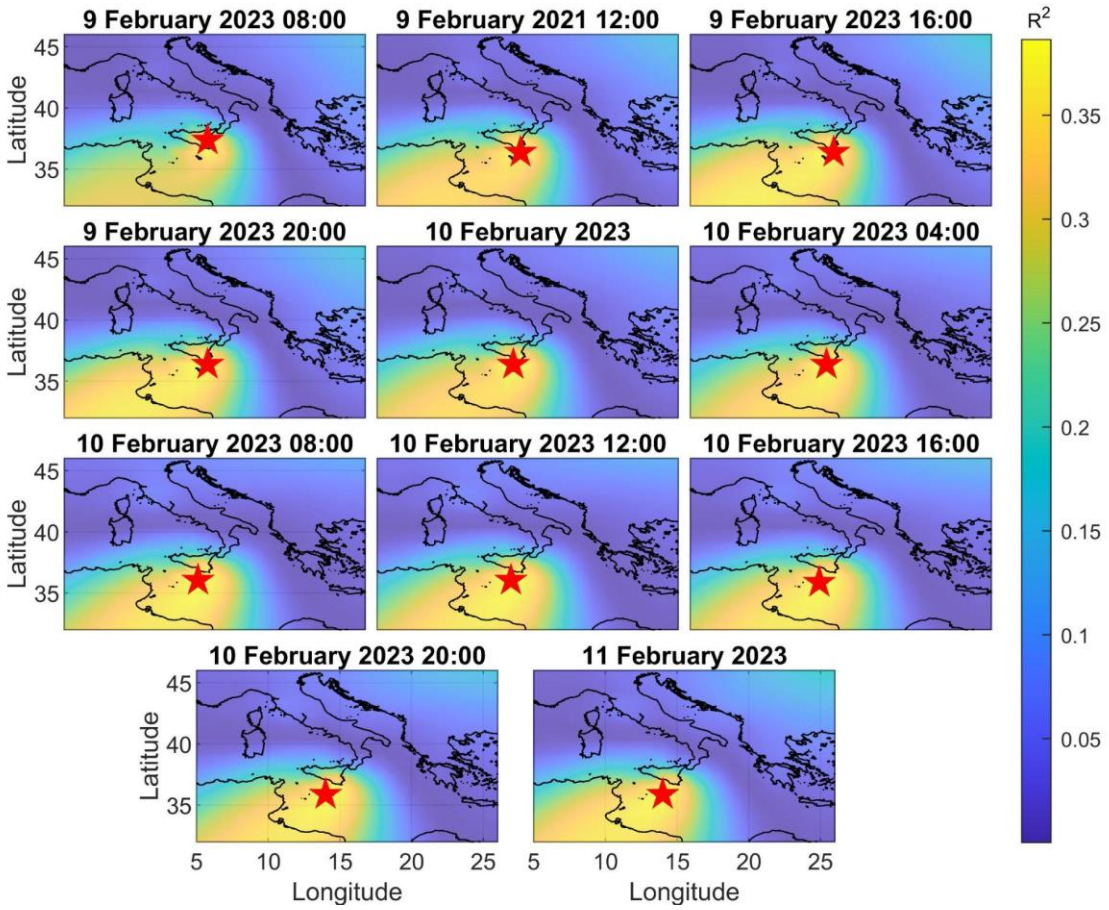

Supplementary Figure ~~6~~7: Spatial distribution of R^2 values during the entire period when we obtained reliable locations. The red five-point star indicates the centroid position of all the grid nodes whose R^2 values do not differ by more than 1% from the maximum R^2 value.

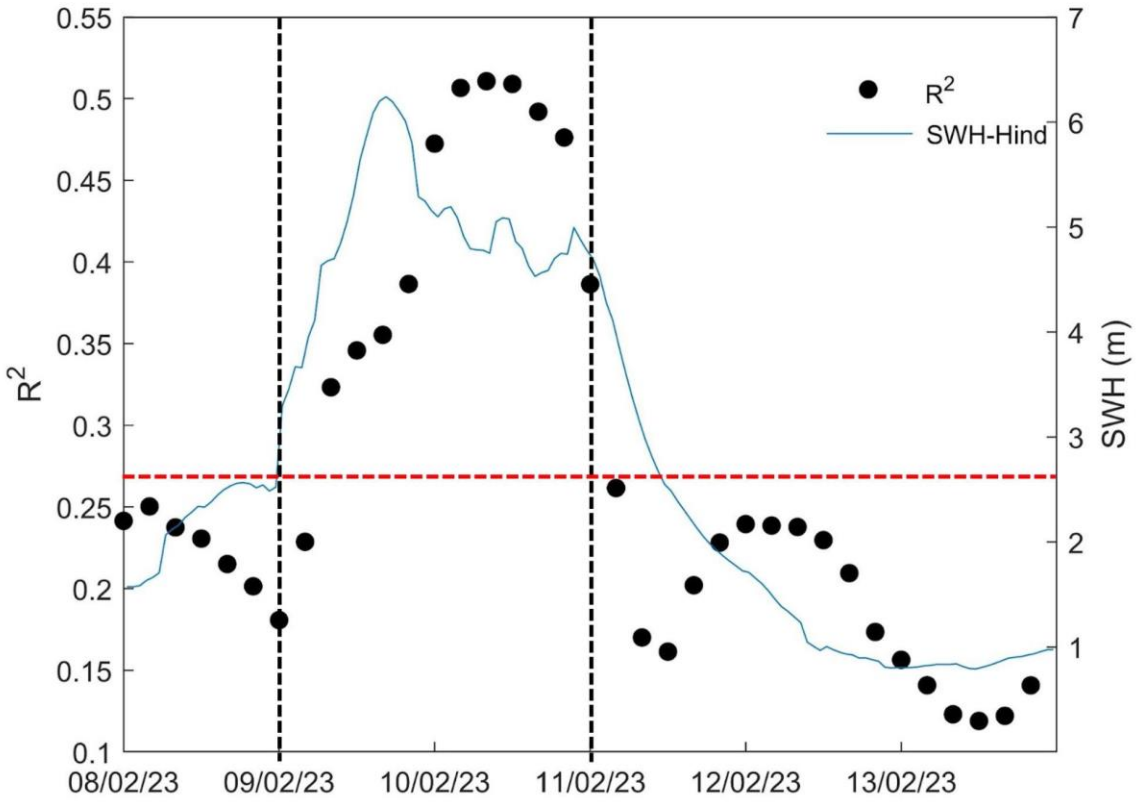

Supplementary Figure ~~7~~8: Scatter plot showing the time series of the maximum R^2, obtained by the location analysis, and of the SWH-Hind, obtained by computing the median value of the SWH data within the area in **Figure 8d** . The black dashed lines represent the time interval when Helios reached its highest intensity while the red dashed line indicates the R^2 reliable threshold.

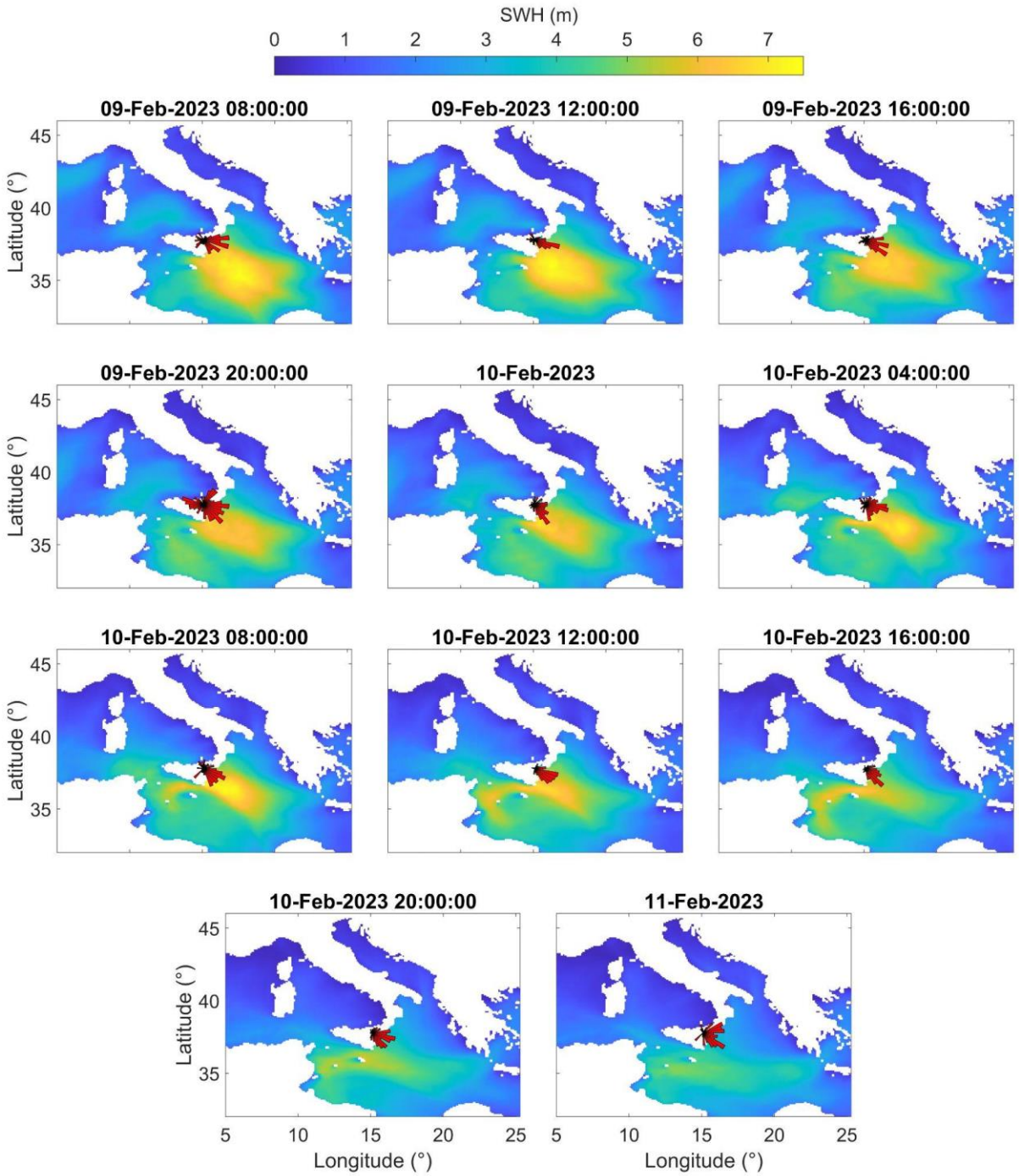

Supplementary Figure ~~8~~9: Hindcast maps showing the significant wave heights (in m) during the entire period when we obtained reliable locations by the grid search method. The rose diagram, located at the center of the Etna seismic permanent network (see **Figure 2b**), shows the distribution of the back azimuth values computed by the f–k analysis for the PM frequency band.

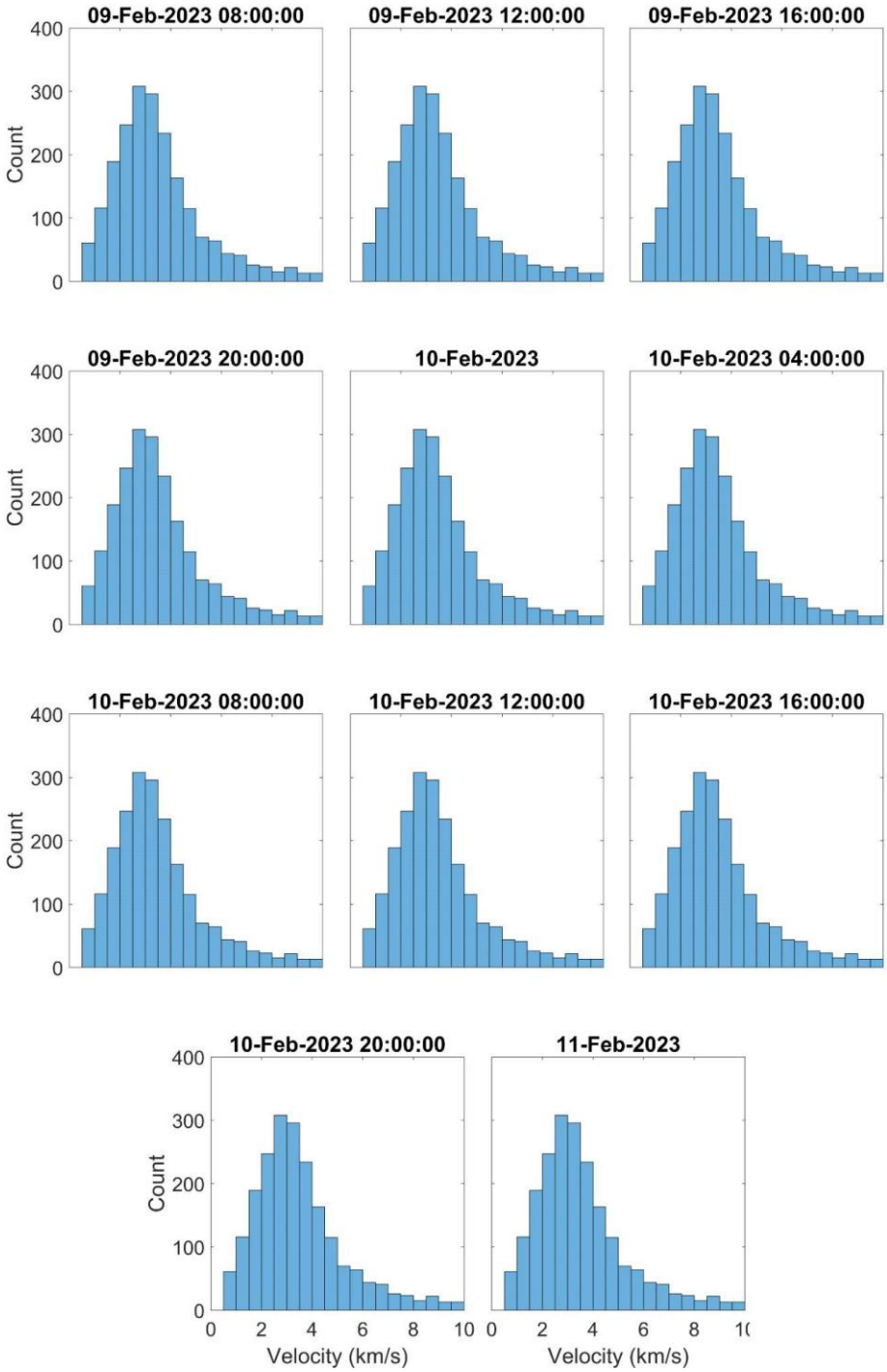

Supplementary Figure ~~9~~10: Distribution of apparent velocity values computed by f-k analysis for the PM frequency band. These values were calculated during the entire period when we obtained reliable locations by the grid search method.

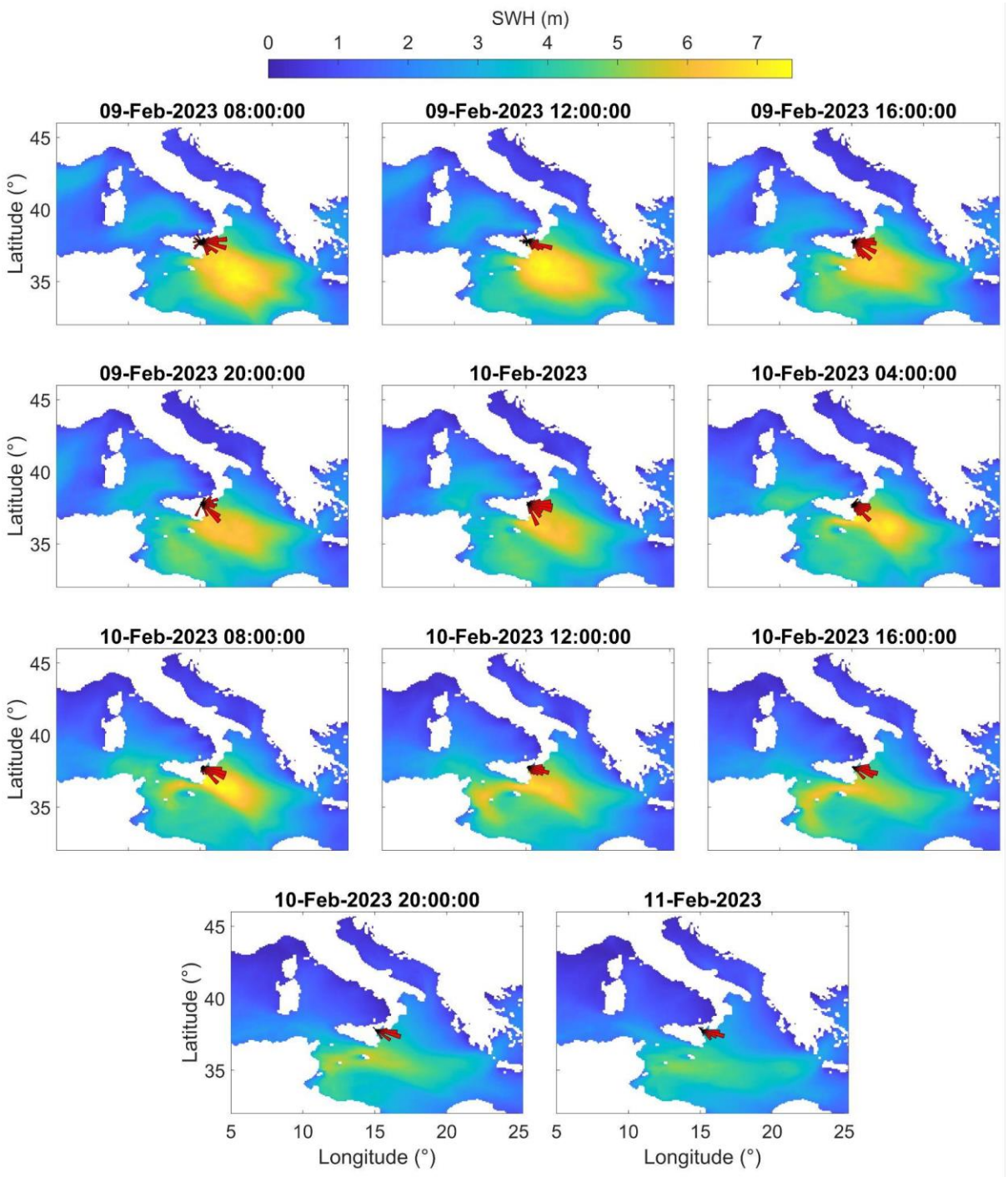

Supplementary figure ~~10~~11: Hindcast maps showing the significant wave heights (in m) during the entire period when we obtained reliable locations by the grid search method. The rose diagram, located at the center of the Etna seismic permanent network (see **Figure 2b**), shows the distribution of the back azimuth values computed by f–k analysis for the SM frequency band.

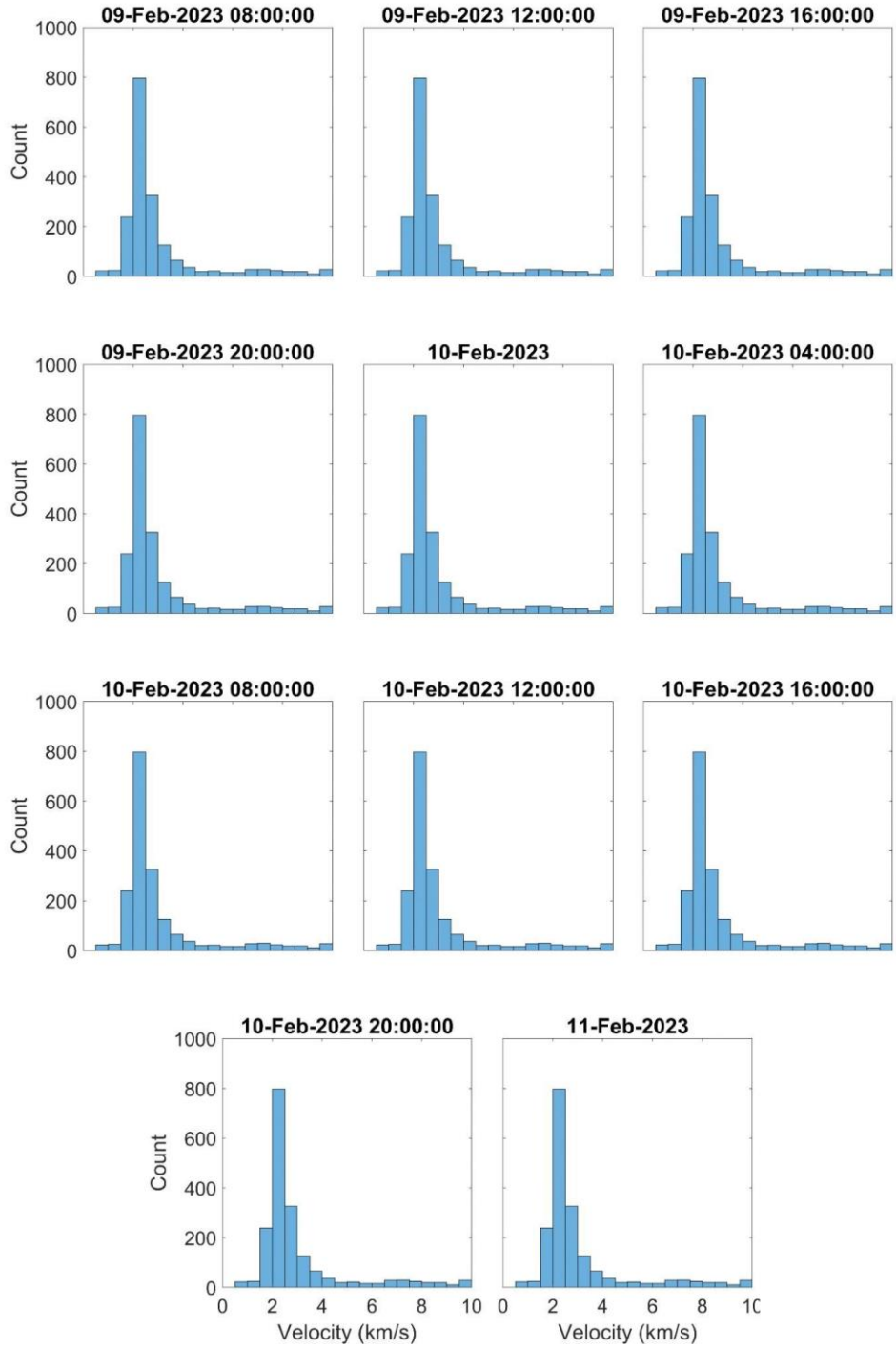

Supplementary Figure ~~11~~12: Distribution of apparent velocity values computed by f-k analysis for the SM frequency band. These values were calculated during the entire period when we obtained reliable locations by the grid search method.